European Journal of Medicinal Chemistry 105 (2015) 274–288

Contents lists available at ScienceDirect

European Journal of Medicinal Chemistry

journal homepage: http://www.elsevier.com/locate/ejmech

Research paper

Design and synthesis of 2-oxindole based multi-targeted inhibitors of PDK1/Akt signaling pathway for the treatment of glioblastoma multiforme

Simona Sestito [a, 1], Giulia Nesi [a, 1], Simona Daniele [a], Alma Martelli [a], Maria Digiacomo [a], Alice Borghini [b], Daniele Pietra [b], Vincenzo Calderone [a], Annalina Lapucci [a], Marco Falasca [c], Paola Parrella [d], Angelantonio Notarangelo [e], Maria C. Breschi [a], Marco Macchia [a], Claudia Martini [a], Simona Rapposelli [a, *]

[a] Department of Pharmacy, University of Pisa, Via Bonanno, 6, 56126 Pisa, Italy
[b] Alidans S.r.l., Via Vecchializia, 48, 56017 San Giuliano Terme, PI, Italy
[c] Metabolic Signalling Group, School of Biomedical Sciences, Curtin Health Innovation Research Institute Biosciences, Curtin University, Perth, Western Australia 6102, Australia
[d] Laboratory of Oncology, Hospital "Casa Sollievo Della Sofferenza", Viale Cappuccini, 1, 71013 San Giovanni Rotondo, FG, Italy
[e] Medical Genetics Unit, IRCCS Casa Sollievo della Sofferenza Hospital, I-71013 San Giovanni Rotondo, FG, Italy

ARTICLE INFO

Article history:
Received 19 August 2015
Received in revised form
5 October 2015
Accepted 8 October 2015
Available online 22 October 2015

Keywords:
PDK1 inhibitors
Kinase inhibitors
Oxindole derivatives
Glioblastoma
GBM stem cells
Multi-target therapy

ABSTRACT

Aggressive behavior and diffuse infiltrative growth are the main features of Glioblastoma multiforme (GBM), together with the high degree of resistance and recurrence. Evidence indicate that GBM-derived stem cells (GSCs), endowed with unlimited proliferative potential, play a critical role in tumor development and maintenance. Among the many signaling pathways involved in maintaining GSC stemness, tumorigenic potential, and anti-apoptotic properties, the PDK1/Akt pathway is a challenging target to develop new potential agents able to affect GBM resistance to chemotherapy. In an effort to find new PDK1/Akt inhibitors, we rationally designed and synthesized a small family of 2-oxindole derivatives. Among them, compound **3** inhibited PDK1 kinase and downstream effectors such as CHK1, GS3Kα and GS3Kβ, which contribute to GCS survival. Compound **3** appeared to be a good tool for studying the role of the PDK1/Akt pathway in GCS self-renewal and tumorigenicity, and might represent the starting point for the development of more potent and *focused* multi-target therapies for GBM.

1. Introduction

Glioblastoma multiforme (GBM) is the most common and lethal primary malignancy of the central nervous system (CNS) with a median survival rate of approximately 14 months [1]. Histologically, it is characterized by poorly differentiated astrocytes, atypical nuclei, intense mitotic activity, vascular thrombosis, microvascular proliferation and necrosis [2,3]. Despite of many efforts to investigate new therapies, there has been little improvement in survival rate over the last 30 years [4]. In addition, evidence indicates that a population of tumor cells, *i.e.* cancer stem cells (CSCs), contributes to cancer recurrence and ultimate failure of the existing therapeutic strategies thus delineating GBM as a hierarchically organized entity [5].

CSCs represent the core of the cancer with great capacity for self-renewal and high level of therapy resistance, suggesting that they should be a pivotal therapeutic target in order to achieve a complete eradication of the tumor itself.

As expected, GBM-derived stem cells (GSCs) display selective resistance to several chemo- and radio-therapies [6]. In particular, irradiated GBMs express an increased level of the stemness marker CD133 compared to non-irradiated ones [7]. The resistance in GSCs may depend on several mechanisms, such as a high expression of drug

Abbreviation: PI3K, phosphatidylinositol-3-kinase; PDK1, phosphoinositide-dependent kinase-1; GSK3, Glycogen synthase kinase 3; CHK1, Checkpoint kinase-1; Akt, protein kinase B; OXIDs, 2-oxindole derivatives; GBM, glioblastoma; GSCs, Glioblastoma-derived stem cells.

* Corresponding author.
E-mail address: simona.rapposelli@farm.unipi.it (S. Rapposelli).

[1] Equally contributed.

http://dx.doi.org/10.1016/j.ejmech.2015.10.020
0223-5234/

efflux pumps [8] and, more importantly, a high DNA repair activity.

Accumulating experiences with targeted therapies in different tumor types clearly indicate that the understanding of the molecular mechanisms of oncogenesis, as well as the correlation of genetic and pathological features, are pivotal in designing more effective personalized treatments. The loss of regulatory mechanisms is the result of alterations in expression of genes involved in cell cycle control, such as proto-oncogenes and tumor suppressor genes [9].

The PI3K/Akt pathway has been identified as an important oncogenic pathway in the malignant phenotype of GBM, because triggers a cascade of downstream signaling events that leads to tumor growth, survival, invasion into normal brain, and secretion of angiogenic factors. In addition, greater activation and deregulation of PI3K/Akt components appears to increase cell proliferation and inhibit GSCs differentiation, thus contributing to resistance to chemotherapy [10].

As a consequence, a plethora of new compounds targeting different nodes of this pathway, such as PI3K inhibitors [11], have been developed, and specific drugs targeting Akt/mTOR are now in Phase I/II of clinical trials, alone or in combination with other chemotherapeutic drugs against GBM [12,13] (Fig. 1).

The increasing understanding of the key role played by PI3K/Akt pathway in resistant cancer phenotype prompted us to design and synthesize a small series of 2-oxindole derivatives able to inhibit Akt phosphorylation [14] (Fig. 1). Noteworthy the oxindole is the central nucleus of different PI3K/Akt pathway inhibitors [15–17]. Starting from these results and aiming to widen the Structure-Activity Relationships (SAR) of this new class of compounds, this study deals with (a) the design and synthesis of new inhibitors of PDK1/Akt pathway, (b) prediction of physicochemical and ADME (Absorption, Distribution, Metabolism, Excretion) properties, (c) selection of lead compound(s) through a screening assay on AKT (PKB alpha) and "PDK1 Direct kinases"(d) characterization of the mechanism of action of selected lead-compound including kinases profiling, and antiproliferative activity on different GBM cell lines and finally (e) exploration of the effects induced on GSCs proliferation and differentiation.

Among the compounds synthesized, the oxindole **3** effectively reduces the viability on two different human glioblastoma cell lines, ANGMS-CSS [18] and U118MG, which are poorly responsive to conventional chemotherapies, such as temozolomide (TMZ). Moreover, compound **3** inhibits GSC self-renewal and proliferation, triggering both apoptosis and differentiation of the stem cell subpopulation. These findings suggest **3** as a novel tool to sensitize GSCs to traditional chemotherapeutic strategies.

2. Results and discussion

2.1. Design and in silico prediction of pharmacokinetic properties

This study started from our recent findings suggesting that 2-oxindole derivatives (OXIDs) inhibit the PDK1/Akt pathway in non-small cell lung cancer (NSCLC) [14]. In order to investigate more deeply this class of compounds, we performed a systematic medicinal chemistry optimization through a divergent synthetic route in three steps. Recent findings demonstrated that the 2-oxindole nucleus may be considered as a valid framework upon

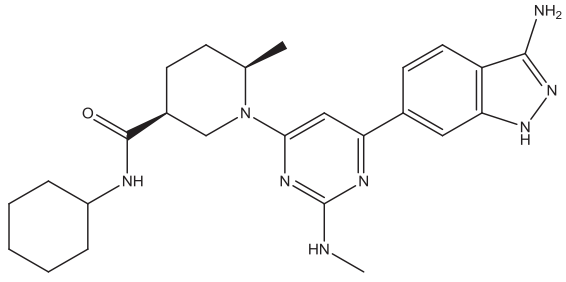

GSK2334470
PDK1Inhibitor

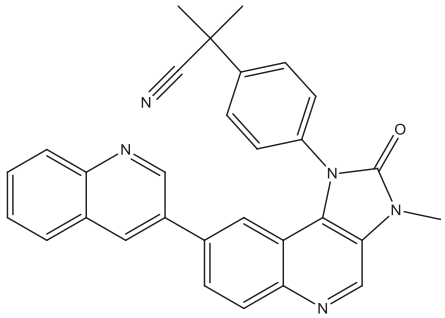

DACTOLISIB
PI3K/mTOR Inhibitor

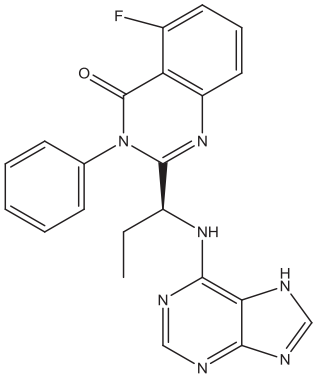

IDEALALIDIB
PI3K Inhibitor

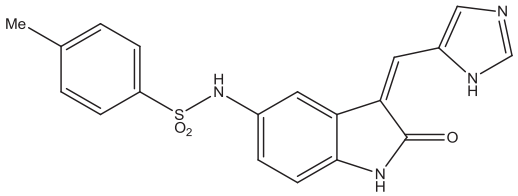

FC85
Akt/mTOR Inhibitor

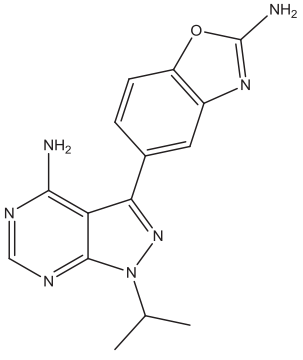

INK128
mTOR Inhibitor

Fig. 1. Structures of PI3K/Akt/mTOR inhibitors.

which to design new ligands able to target the PI3K/Akt. Moreover, the substituent in 5-position seems to play a detrimental role for the affinity against different kinases involved in the PI3K/Akt pathway [19]. In particular, the substitution of 3,4-dimethoxytetrahydroisoquinoline alkylamido side chain of previously synthesized oxindole derivatives [14] with a tolylsulfonamido group, led to dual Akt/mTOR inhibitors such as FC85 [19] (Fig. 1). On these basis, we planned to study more deeply the effects induced by the substituent in 5-position on the affinity against PDK1 and Akt kinases. Hence, herein we first explore the 5-position of OXID-framework by the substitution of 3,4-dimethoxytetra hydroisoquinoline-N-acetamide side chain of **1**–**3** with a group showing greater flexibility and conformational freedom such as 3,4-dimethoxybenzylamino-N-acetamide moiety (**4**). Then, we replaced the substituent in 5-position with an electron-rich linker such as the arylurea- (**5**–**10**) and arylmethyleneamino-sulfonyl moieties (**11**–**13**), or with a lesser hindered group, such as the methanesulphonylamido ones (**14**–**16**).

Since a fast and trustworthy prediction of biological properties is a key factor to accelerate the process of drug discovery, we estimated *in silico* the main numerical and topological indices together with the molecular transport properties (i.e. blood brain barrier penetration) by PaDEL Descriptor [20] (MW, nHBA, nHBD, nRotB, nRotBt, and LipinskiFailures) and by ChemAxon MarvinSketch 6.3.0 (LogP, LogD, TPSA, and pKa) [21]. Moreover, based on aforementioned calculated molecular features, a druglikeness central nervous system multiparameter optimization (CNS MPO) algorithm recently published by Wager et al. [22] was applied to compounds under investigation. The CNS MPO desirability score for CNS drugs should be $\geq$4 on 0–6 scale. According to the Lipinski's rule, molecules with good membrane permeability have Log*P* $\leq$5, molecular weight $\leq$500, number of hydrogen bond acceptors $\leq$10, and number of hydrogen bond donors $\leq$5. On the basis of the calculated values (Table 1), we synthesized the designed compounds since all molecules seemed to satisfy the Lipinsky's rule of five [23].

2.2. Synthesis of new OXID-derivatives

The final compounds **1**–**3** were synthesised as previously reported [14,19] whereas compounds **4**–**10** were obtained following the synthetic procedure illustrated in Scheme 1. The catalytic reduction of 5-nitro-2-oxindole gave the 5-amino-2-oxindole **17** which was then reacted with 4-(methylthio)phenyl-isocyanate providing the ureido-intermediate **18**. The subsequent Knoevenagel reaction with the appropriate carbaldehydes gave the compounds **5**–**7**. Oxidation of **5**–**7** with Oxone® ($KHSO_5 \cdots 0.5\ KHSO_4 \cdots 0.5\ K_2SO_4$) in MeOH-THF yielded to final products **8**–**10**. The 5-amino-2-oxo-indole **17** was also submitted to a reaction with methanesulfonyl chloride affording methansulphonamido intermediate **19**, which was reacted with thiophene-2-carbaldehyde, (N-methyl)-imidazole-2-carbaldehyde or 1*H*-imidazole-5-carbaldehyde affording compounds **14**–**16**, respectively. Finally, starting from intermediate **21**, easily obtained by a nucleophilic substitution of the α-chloroacetamido-derivative **20** with the 3,4-dimethoxybenzylamine, the reaction with thiophene-2-carbaldehyde gave the final product **4**.

The arylmethyleneamino-sulfonyl derivatives **11**–**13** were obtained starting from 2-oxo-indole **22**. (Scheme 2). Derivative **22** was obtained by a handy and efficient one-pot reductive cyclization of 2-nitrophenylacetic acid with iron and acetic acid [24]. The following reaction with chlorosulphonic acid gave the 5-(chlorosulfonyl)indolin-2-one **23** as intermediate which reacted with 3,4-dimethoxybenzyamine affording the adduct **24**. Finally, the Knoevenagel reaction with the appropriate carbaldehyde gave final product **11**–**13**.

An analysis of NMR spectra allowed us to assign the configuration around the double bond in 3-position of the OXID core. In particular, the final 3-(*1H*-imidazole-5-yl)-adducts (**3**,**7**,**10** and **13**) exist exclusively as *Z*-isomers, whereas the OXID-derivatives substituted in 3-position with N-methyl-imidazol-2-yl moiety (**2**, **6**, **9**, **12**) preferentially adopt the *E*-isomeric form [25].

On the contrary, we observed that the 2-thienyl substituted products exist as E/Z mixture even if a sharp prevalence of Z-isomer has been observed.

2.3. Pharmacology

2.3.1. Effects induced on ASPC1 cell viability

For a preliminary evaluation of the cytotoxicity of the synthesized compounds **1**–**16**, we decided to use the ASPC1 cells [26]. This human pancreatic adenocarcinoma cell line is an appropriate model to study new inhibitors of PI3K-AKT pathway, since: i) it is characterized by an aberrant activation of PI3K/Akt pathway and ii) shows high degree of resistance to currently available chemotherapeutic drugs [27] and to PI3K inhibitors [26].

All the compounds synthesised (**1**–**16**) were tested in triplicate at a concentration of 10 μM for 72 h (Table 2). The results show that, within the 2-oxindoles displaying the 3,4-dimethoxytetra hydroisoquinoline alkylamido side chain in 5-position, only compound **3** reduces the cell viability to around 68%. The substitution of this moiety with the thiomethylphenylureido- (**5**–**7**) or with the methylsulphonylphenylureido-groups (**8**–**10**) is deleterious for the activity against the ASPC1, whereas the replacement with a small electron rich group such as the methanesulphonamido group (**14**–**16**), affects only slightly the cell viability compared to compound **3** (ASPC1 cell viability of 68% and 74% for **14** and **16**, respectively). On the contrary, the replacement of the 3,4-dimethoxytetrahydroisoquinoline-N-acetamide side chain with a substituent endowed of a greater flexibility and conformational freedom such as the 3,4-dimethoxybenzylamino-N-acetamido moiety (**4**) or with the 3,4-dimethoxyaminosulphonyl group (**11**–**13**), induces a decrease of the antiproliferative activity ($\approx$85% cell viability). Bearing in mind the high resistance to conventional therapy reported for the AsPC1 cell line, the reduction of the proliferative activity of around 30% induced by compounds **3**, **14** and **16** prompted us to further investigate them on PDK1/Akt pathway.

2.3.2. In vitro screening assay on Akt and PDK1 enzymes

Because we focused on the discovery of new molecules able to affect the PDK1/Akt pathway, the selected OXID-derivatives **3**, **14** and **16** were consequently submitted to a screening assay on AKT (PKB alpha) and PDK1 direct kinases [28]. Compounds **3, 14** and **16** displayed an appreciable inhibitory activity on PDK1 with IC_{50} values in the micromolar (**14**: $IC_{50} = 6.81$ μM) and submicromolar ranges (**3** and **16**: $IC_{50} = 0.98$ and 0.31 μM, respectively), whereas no inhibition on the recombinant Akt enzyme was observed. The data shows that the replacement of the tetrahydroisoquinoline nucleus in 5-position of the oxindole core (**3**), with the methanesulphonamido chain (**16**) seems not to affect the PDK1-affinity. On the contrary, the substitution of the imidazole in 3-position of **16**, with a thiophene (**14**), dramatically reduced the potency of about 7 folds. This let us to speculate that the decrease of potency could depend, at least in part, to the existence of **14** as a mixture of E/Z-isomers.

2.3.3. In vitro activity on GBM cell lines

In order to establish the *proof of concept* for the development of Akt-PDK1 inhibitors for GBM, compound **3** was selected and investigated on two different human GBM cell lines (ANGMS-CSS and U118MG). These human cell lines show an aberrant activation

Table 1
Molecular descriptors related to ADME and drug-likeness properties of the investigated compounds.

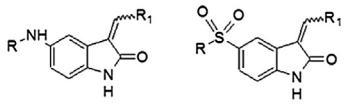

Compd	R	R_1	MW[b]	nHBA[b]	nHBD[b]	nRotB[b]	nRotBt[b]	LogP[c]	LogD[c]	TPSA[c]	pKa[c]	LF	CNS MPO[d]
1[a]	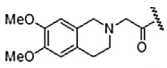		475.56	9	2	7.0	9.0	3.76	3.74	108.14	6.04	0	2.77
2[a]	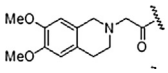		473.52	10	2	7.0	10.0	2.17	2.13	97.72	5.81	0	4.31
3[a]	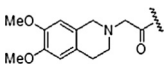		459.50	10	2	7.0	9.0	1.82	1.81	105.68	2.75	0	4.18
4	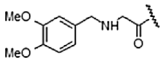		449.52	7	3	9.0	11.0	3.33	2.65	121.51	7.98	0	3.06
5	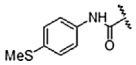		407.51	6	3	6.0	7.0	4.95	4.95	123.77	11.14	0	0.74
6	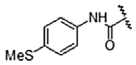		405.47	7	3	6.0	8.0	3.06	3.03	113.33	6.5	0	3.40
7	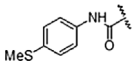		391.45	7	3	6.0	7.0	3.02	3.02	121.31	2.75	0	3.27
8	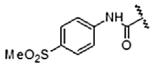		439.51	7	3	6.0	7.0	3.16	3.16	140.99	10.93	0	1.89
9	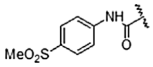		437.47	9	3	6.0	8.0	1.28	1.24	130.57	6.5	0	3.56
10	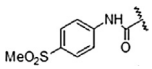		423.44	9	3	6.0	7.0	1.23	1.23	138.53	2.75	0	3.63
11	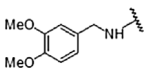		456.53	7	2	7.0	9.0	3.42	3.42	130.35	10.07	0	1.80
12	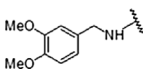		454.50	9	2	7.0	10.0	1.83	1.81	119.93	6.19	0	3.73
13	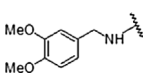		440.47	9	2	7.0	9.0	2.12	2.12	127.89	2.5	0	3.74
14	$MeSO_2$		320.39	5	2	3.0	4.0	1.55	1.55	111.89	9.61	0	3.87
15	$MeSO_2$		318.35	7	2	3.0	5.0	−0.03	−0.06	101.47	6.19	0	5.03
16	$MeSO_2$		304.32	7	2	3.0	4.0	0.44	0.44	109.43	2.5	0	4.83

MW = molecular weight; nHBA: number of Hydrogen Bond Acceptors; nHBD: number of Hydrogen Bond Donors; nRotB: Rotational Bonds; nRotBt: terminal Rotational bonds; LogP = partition coefficient; LogD = distribution coefficient; TPSA = topological polar surface area; pKa = most basic center; LF (Lipinski failures) = number of deviations from Lipinski's rule; CNS MPO = druglikeness central nervous system multiparameter optimization.
[a] Ref. [10].
[b] Calculated with PaDEL descriptors.
[c] Calculated with MarvinSketch.
[d] Calculated according to Ref. [13].

of PDK1/Akt pathway due to PTEN mutation [18,29] and are also characterized by a high grade of resistance against TMZ, an alkylating agent widely used to treat GBM. The selection of the oxindole **3** as prototype to further investigate in GBM cells has been driven by (a) the satisfactory and repeatable effect recorded on ASPC1 cells (Table 2), (b) the predicted ability to penetrate the blood–brain barrier (BBB) (Table 1) and (c) the significant cytotoxicity previously showed in the A549 cell line, which has been reported to be

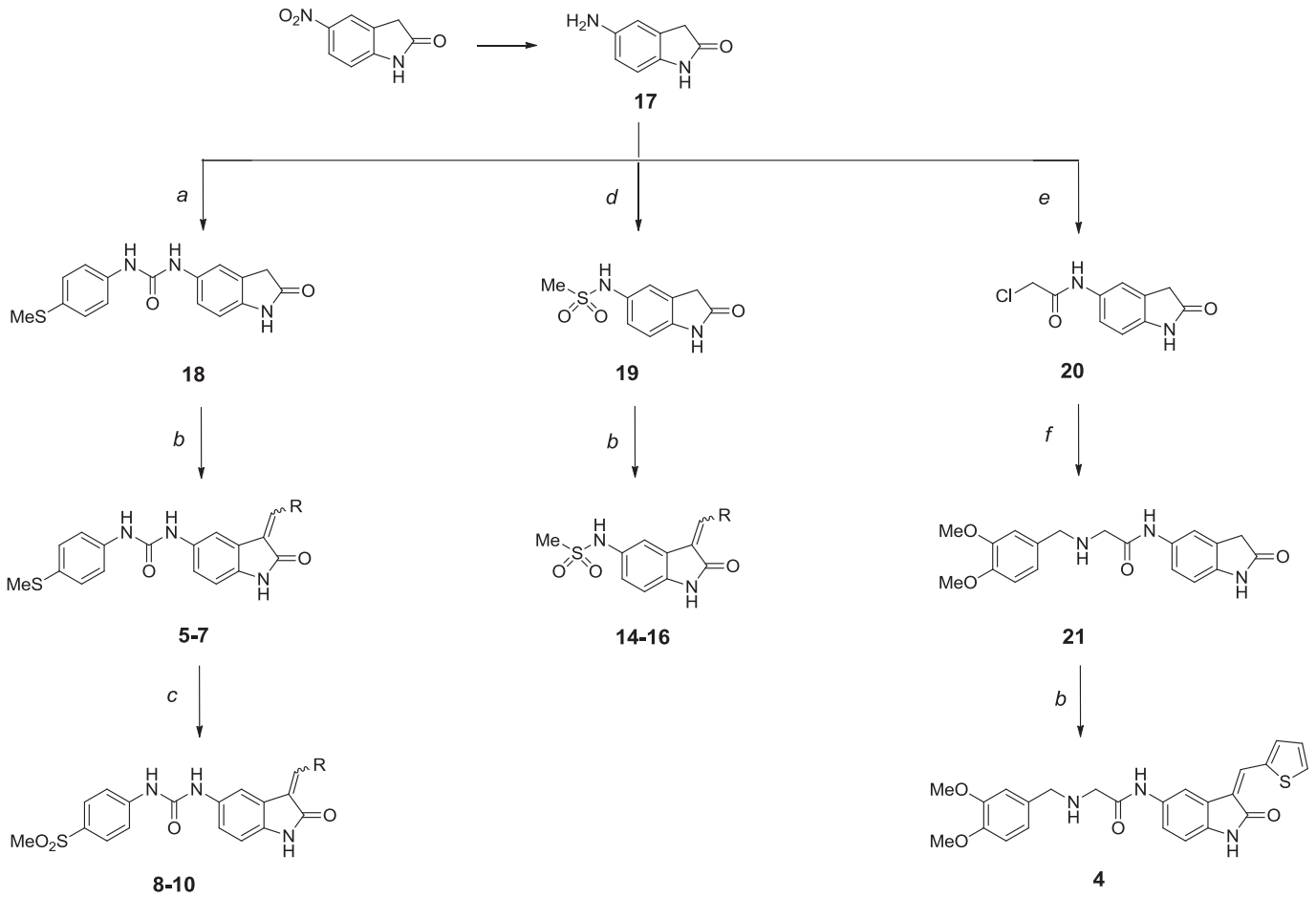

Compd	R	Compd	R	Compd	R
5,8,14		6,9,15		7,10,16	

Scheme 1. [a]. **Reagents and conditions**. *a)* (methylthio)phenyl-isocyanate, DCM/MeOH, 10°C–rt, 3–4 h; *b)* Aryl-carbaldehyde, EtOH, piperidine, 110 °C, 12 h; *c)* Oxone, MeOH/THF, rt, 12 h; *d)* MsCl, H_2O, rt; *e)* $ClCH_2COCl$, H_2O, rt, 3 h; *f)* 3,4-Dimethoxybenzylamine, K_2CO_3, DMF, CH_3CN, 82 °C, 12 h.

gefitinib-resistant due to the maintenance of an EGFR-independent activity of the PI3K/Akt pathway [14]. Actually, considering the in vitro PDK1 inhibitory activity, the antiproliferative activity on ASPC1 cell line and the CNS MPO score of 4.2, the oxindole **3** was selected as the best candidate.

Consequently, the antiproliferative effects induced by **3** derivative on GBM cell lines was also assessed. Noteworthy, both ANGM-CSS and U-118MG cell lines showed to be unresponsive to the treatment with 100 μM of TMZ for 72 h (data not shown). Compound **3** was tested at different concentrations for 72, 96, 120 and 144 h (Fig. 2). Data show that **3** inhibits cell growth in a concentration-dependent manner, in both cell lines with GI_{50} values in the low micromolar range (Fig. 2). Among the two cell lines, ANGM-CSS appears to be more responsive than U-118MG.

Treating the cells for 72 h with **3** (10 μM) caused a significant amount of phosphatidylserine externalisation, in the absence of 7-AAD binding to DNA (Fig. 3A and B), demonstrating that the compound induced early and late apoptosis of ANGM-CSS cells. As depicted in Fig. 3 (panels C and D) compound **3** induced cell cycle disturbance, strongly arresting cell-cycle in the G0-G1 phase.

The significant reduction of cell viability and the proapoptotic effect of **3** in both resistance cell lines suggest a possible contribution of "off-target" activities. Indeed, PDK1 inhibition has been proposed as a highly effective mechanism for reducing metastasis propagation, but also as an unable mechanism, at least as selective PDK1 inhibitor, in reducing proliferation in cancer cells characterized by an aberrant PI3K/PDK1/AKT expression [30]. Therefore, to elucidate the mechanism of action of OXID-derivative **3**, a screening profile on 60 kinases involved in the PI3K/Akt/mTOR pathway was performed.

2.3.4. SelectScreen kinase profiling

The study was carried out by SelectScreen Kinase Profiling Service, Invitrogen-Life Technologies. Among almost 60 protein kinases screened, compound **3** (1 μM) showed a high inhibitory activity towards GSK3 beta (70% inhibition), a significant activity towards GSK3 alpha and CHK1 (59% and 61%, respectively) (Table S1 Supporting Information) and a low activity towards ABL1 (55%). Compound **3** modestly inhibited (<45%) any of all the other tested kinases, including members of both the PKC family (i.e

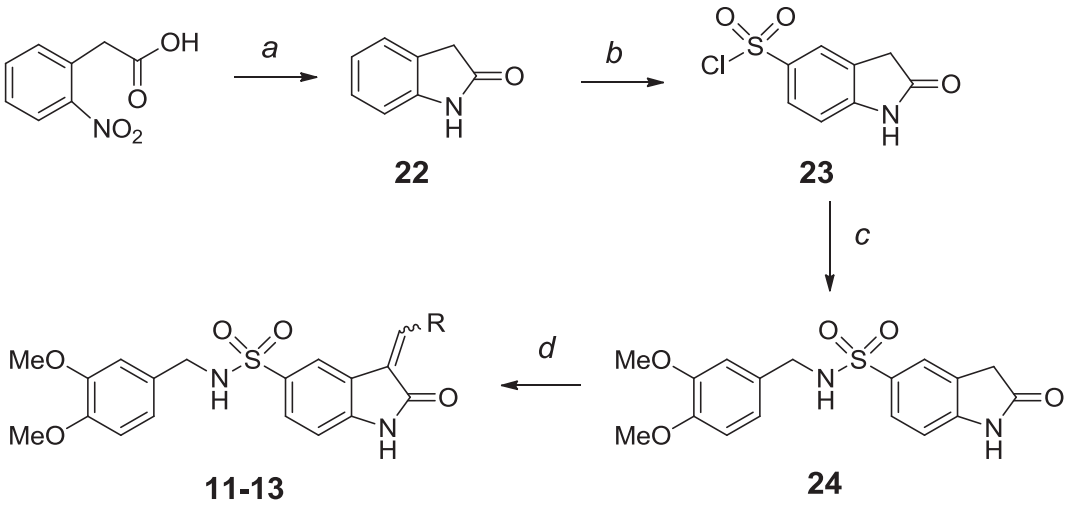

Compd	R	Compd	R	Compd	R
11	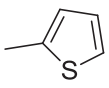	12	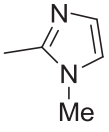	13	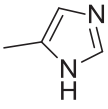

Scheme 2. [a]. Reagents and conditions. *a)* Fe, AcOH, reflux, 2 h; *b)* $ClSO_2OH$, rt, 1.5 h → 68 °C, 1 h; *c)* 3,4-dimethoxybenzylamine, EtOH, rt, 4 h; *d)* Aryl-carbaldehyde, EtOH, pirrolidine, 110 °C.

Table 2
Cytotoxicity of compounds **1**–**16** on ASPC1 cell proliferation assessed by cell counting at 10 μM after 72 h (% viable cells compared to control). Data were expressed as mean values ± SEM (n = 3).

Compd	Cell counting ±S.D.	Compd	Cell counting ±S.D.
1	82.04 ± 3.44	**9**	90.57 ± 3.88
2	82.34 ± 2.87	**10**	82.21 ± 9.43
3[a]	*68.14 ± 2.23*	**11**	84.18 ± 6.67
4	86.75 ± 0.76	**12**	84.50 ± 4.75
5	77.29 ± 9.93	**13**	n.d.
6	95.13 ± 3.46	**14**[a]	*68.06 ± 11.08*
7	82.94 ± 1.42	**15**	96.23 ± 3.55
8	93.88 ± 5.53	**16**[a]	*73.83 ± 11.19*

[a] Reduction of the proliferative activity of around 30%.

AMPK) and the MAPK family (i.e. ERK, JNK). These data indicate that **3** inhibits PDK1 with IC_{50} 980 nM and that, at this concentration (1 μM) it possesses also a high inhibitory activity towards CHK1 and GSK3A and GSK3B, exhibiting IC_{50} values in the micromolar/sub-micromolar (Table 3). These data revealed that OXID-derivative **3** is a novel *focused* multi-target PDK1/Akt pathway inhibitor.

2.3.5. *Effects of 3 on GSC proliferation*

Recent evidences demonstrate that GSK-3 inhibition can inhibit proliferation and induce differentiation of GSCs [31]; moreover, a combined PDK1 and CHK1 inhibition has been reported to play a pivotal role in GSC apoptosis [32]. These findings suggest that the simultaneous inhibition of GSK-3, PDK1 and CHK1 may deplete the GBM stem cell reservoir. Accordingly, **3** was characterized on GSCs, isolated from glioblastoma ANGM-CSS cells as previously reported [19,33].

The OXID-compound induced a time-dependent inhibition of GSC proliferation (Fig. 4). Moreover, the anti-proliferative effects appeared to be concentration-dependent, with an IC_{50} value of 530 ± 48 nM after 7 days of incubation (Fig. 4).

2.3.6. *Effects of 3 on GSC apoptosis and cell cycle block*

We then investigated whether the reduction of GSC proliferation elicited by **3** could be associated to apoptosis. Treating GSC with **3** for 7 days caused a significant phosphatidylserine externalization in the absence of 7-amino-actinomysin binding to DNA, thus denoting the induction of early apoptosis (Fig. 5). In addition, cell cycle analysis demonstrated that challenging GSCs for 7 days with **3** induced a slight cell cycle disturbance, arresting cell-cycle progression in the G2-M phase (Fig. 5), consistent with a CHK1 inhibition [19].

2.3.7. *Effects of 3 on morphology and differentiation of GSCs*

The effect of **3** on GSC morphology was evaluated quantifying the area occupied by the cells in culture plates, as well as the outgrowth of cellular processes. Representative photographs of control and treated cells are shown in Fig. 6. Compound **3** reduced the area occupied by the floating spheres after 7 days of GSC treatment, and led to a prominent outgrowth of cellular processes (Fig. 6), suggesting that the compound could also induce GSC differentiation. To confirm this hypothesis, the levels of stem and differentiation markers upon stimulation with **3** were assessed by Real Time RT-PCR analysis. In GSCs treated with **3** a significant

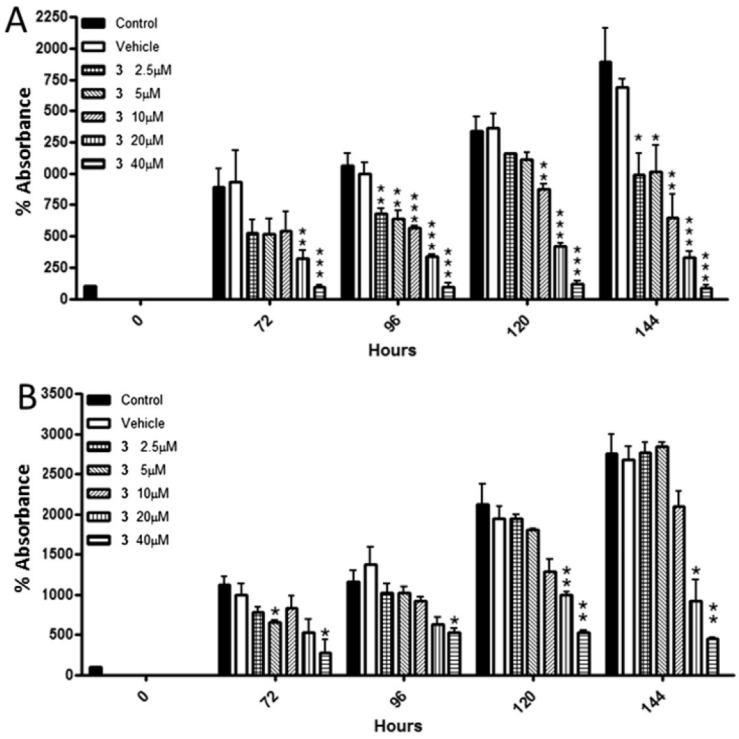

h	GI_{50} (μM)
144	3.98
120	12.88
96	7.50
72	7.73

h	GI_{50} (μM)
144	16.15
120	16.66
96	29.93
72	14.56

Fig. 2. Histograms represent cell viability on ANGM-CSS cell line (A) and U118MG (B) after 72, 96, 120 and 144 h of no treatment (Control), treatment with several concentrations of compound **3** (2.5, 5, 10, 20, 40 μM) or vehicle (DMSO 0.1%). The GI_{50} values recorded at each time, are also shown. Vertical bars indicate the standard error. The asterisk (*) indicates a value of viability significantly different from the value of viability of the corresponding control group (*P < 0.05; **P < 0.01; ***P < 0.001).

decrease in the stemness markers, CD133 and Nestin, was noticed, accompanied by a significant increase of Olig, MAP2 and GFAP content. These data demonstrate that the compound was able to promote GSC differentiation toward a neuronal and a glial phenotype. Comparing the morphological analysis and RT-PCR data indicated that the compound triggered both apoptosis and differentiation of GSCs.

2.3.8. Effects of 3 on the formation of GSCs

Next, on the light of GSK3's role in GSC self-renewal [31], the ability of **3** to affect the formation of GSCs was examined. To this purpose, adherent ANGM-CSS cells were switched to a defined serum-free NSC medium, and cells were allowed to growth for 9 days, in the absence or in the presence of **3**. As depicted in Fig. 7, **3** reduced the number and the diameter of newly generated neurospheres. These results confirmed the importance of GSK3 not only in the maintenance of cancer stem profile, but also in their transformation process.

3. Conclusion

Since the aberrant activation of the PDK1/Akt pathway has been reported as a pivotal player in many cancer types as well as in the stem cell subpopulation, the possibility to develop new molecules that target different steps involved in (and/or downstream of) this signaling system, represents a novel strategy to improve the treatment outcome.

The compelling need to develop new and more effective therapies for the treatment of unresponsive tumors such as GBM, prompted us to design and synthesized new inhibitors of PDK1/Akt pathway. Recent findings demonstrated that 2-oxindole nucleus may be considered as a good starting point to be optimized in order to obtain new targeted ligands. Hence, in this paper we described the synthesis and the in vitro evaluation of a small family of OXID-derivatives (1–16). Among the new compounds, **3** showed to be a good candidate to further investigate in chemoresistant GBM cell lines, because it proved to have: i) a CNS MPO score ≥4 (requirement for CNS drugs); ii) a significant cytotoxicity against a high resistant cell line (ASPC1), in which the pathway is aberrantly expressed, and iii) it inhibited PDK1 kinase, as well as some downstream effectors such as CHK1, GS3Kα and GS3Kβ.

Aiming at establish the *proof of concept* for the development of Akt-PDK1 inhibitors for GBM, compound **3** was investigated on different human glioblastoma cell lines: ANGMS-CSS and U118MG. Results showed that compound **3** proved to induce a concentration-dependent inhibition of cell growth in both cell lines, even if ANGM-CSS appears to be more responsive than U-118MG. Therefore, considering the significant antiproliferative effect of compound **3** (GI_{50} = 7.73 μM in ANGCSS and GI_{50} = 14.6 μM at 72 h U118MG) with respect to TMZ on both cell lines, we hypothesized that the whole cytotoxic effects resulted from a synergic inhibition of other upstream and/or downstream effectors of PDK1 enzyme. In order to validate such hypothesis and to determine the mechanism responsible for the higher activity on GBM cell lines, a kinase profiling assay has been performed.

Most importantly, **3** inhibited GSC self-renewal and proliferation, confirming that a combined inhibition of PDK1 and CHK1 can represent an effective therapeutic approach to reduce the growth of human GBM [32]. Moreover, OXID **3** promoted GSC differentiation toward a neuronal and a glial phenotype. This effect could be due, at least in part to the inhibition GSK3β [31].

In the whole, compound **3** appears to be a good tool to inhibit GBM proceeding, also inducing stem cell differentiation, by the inhibition of PDK1/Akt pathway involved in promoting tumor growth and thus contributing to anticancer therapy resistance [19]. The OXID-derivative **3** could mark the first step towards the

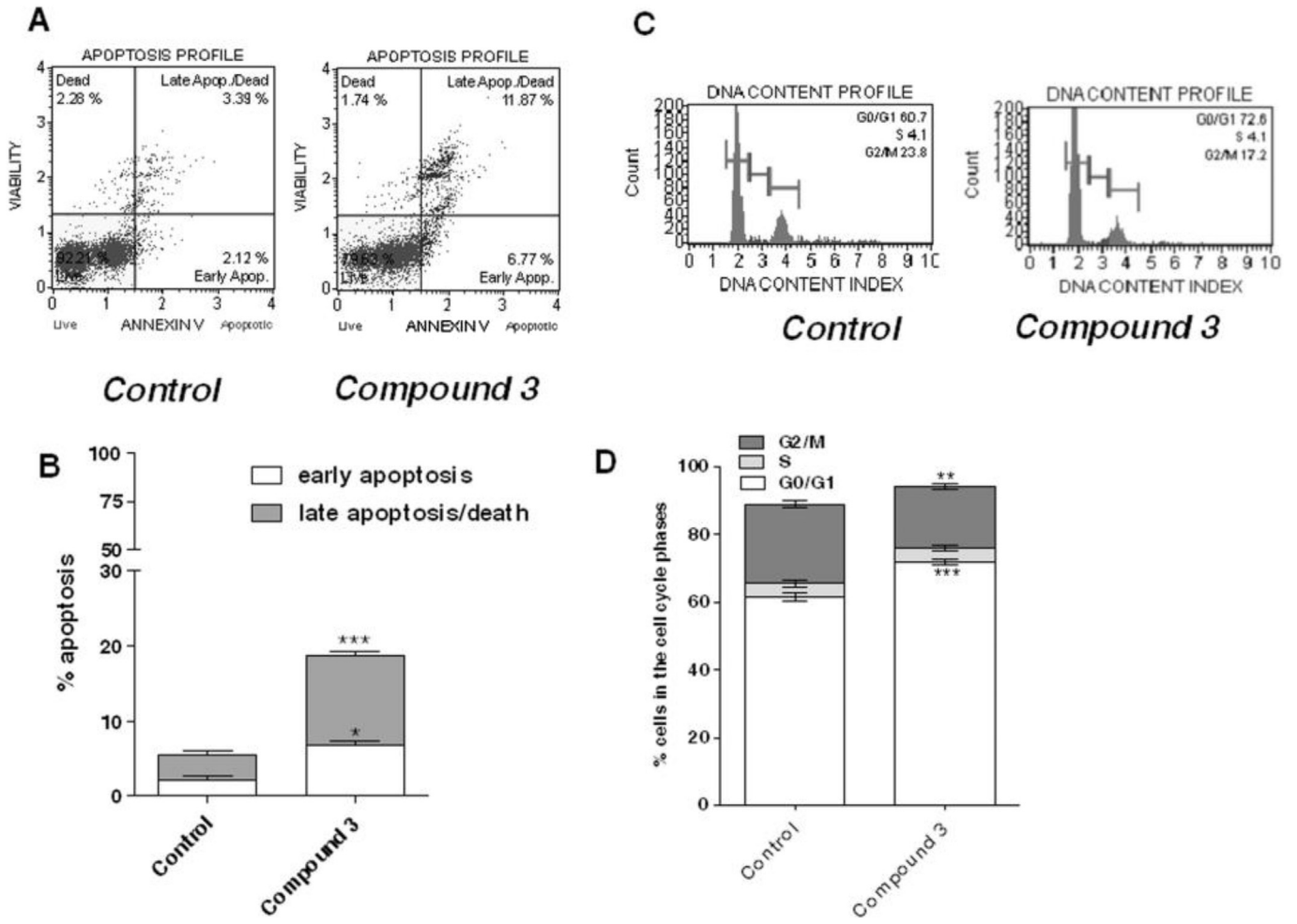

Fig. 3. Compound **3** induced apoptosis and cell cycle arrest. A) ANGM-CSS cells were treated for 72 h with DMSO (control), or **3** (10 μM). At the end of the treatment period, the cells were collected, and the level of phosphatidylserine externalisation was evaluated using the Annexin V-staining protocol. B) The data are expressed as the percentage of apoptotic cells (the data for the early-stage apoptotic cells shown in white, while the ones for the late-stage apoptotic/necrotic cells shown in grey) versus the total number of cells. C, D) ANGM-CSS were treated as in A; at the end of the treatment period, cells were collected and the cell cycle was analyzed. The data were expressed as percentage of cell in the different phases (G0/G1, G2 or S) versus total cell number. All the data shown represent the mean ± SEM of three different experiments. The significance of the differences was determined with a one-way ANOVA with Bonferroni post-test: *$p < 0.05$, **$p < 0.01$, ***$p < 0.001$ vs. control.

Table 3
Results from SelectScreen kinase profiling service (Invitrogen-LifeTechnologies) of **3**.

[ATP] tested (μM)	Kinase	IC_{50}(nM)
10	CHEK1 (CHK1)	274
10	GS3KA (GS3K alpha)	884
10	GS3KB (GS3K beta)	272
25	PDK1 direct	998

development of new *focused* multi-target inhibitors useful in countering the proliferation of GBM cell lines and of their stem cell subpopulation.

4. Experimental procedures

4.1. Chemistry

Chemical shifts (δ) are reported in parts per million downfield from tetramethylsilane and referenced from solvent references. Coupling constants (*J*) are given in Hz. ^{1}H NMR and ^{13}C NMR spectra of all compounds were obtained with a Varian Gemini 200 spectrometer operating at 200 MHz or Bruker TopSpin 3.2 spectrometer operating at 400 MHz, in a ~2% solution of DMSO-d_6, unless otherwise stated. The >95% purity of tested compounds was confirmed by combustion analysis. Reactions were followed by thin-layer chromatography (TLC) on Merck aluminum silica gel (60 F_{254}) sheets that were visualized under a UV lamp. Melting points were determined on a Kofler hot-stage apparatus and are uncorrected. The elemental compositions of the compounds (C, H, N) agreed to within (±) 0.4% of the theoretical values. When the elemental analysis is not included, compounds were used in the next step without further purification. Evaporation was performed in vacuo (rotating evaporator). Sodium sulfate was always used as the drying agent. Celite® 545 was used as filter agent. Commercially available chemicals were purchased from Sigma–Aldrich. Compounds **1**–**3** were synthesized as previously reported [14].

4.2. Procedure for the synthesis of final compounds **4**–**7**

To a solution of 5-substituted-2-oxoindole (0.39 mmol) in EtOH (7 mL) was added the appropriate carbaldehyde (0.43 mmol) and a catalytic amount of piperidine. The resulting solution was stirred and refluxed for 12 h, then the solution was evaporated to dryness.

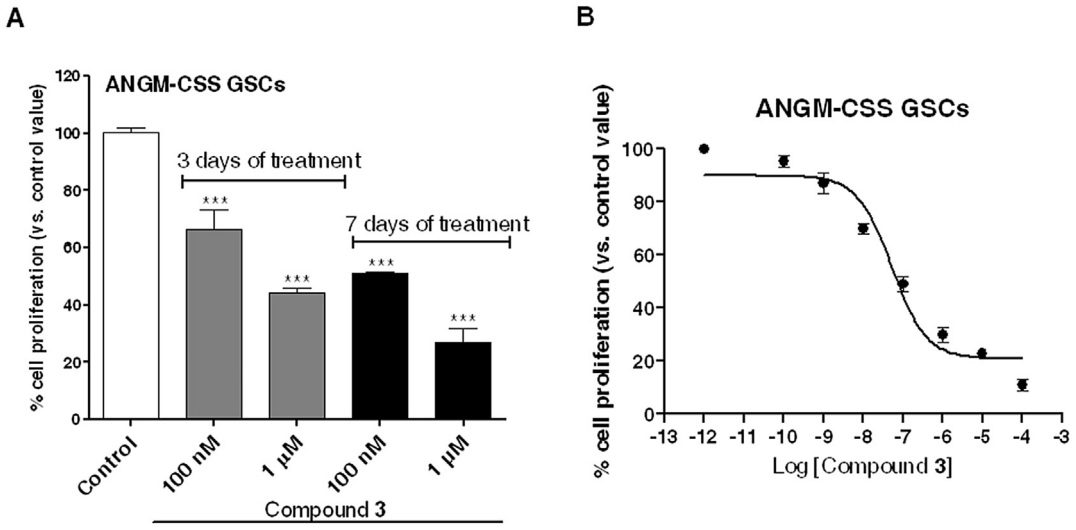

Fig. 4. ANGM-CSS-derived GSCs were incubated in Neural Stem Cells (NSC) medium with the indicated concentrations of **3** for three (A) or seven days (A, B). At the end of the treatment periods, cell proliferation was measured using the MTS assay. The data are expressed as a percentage with respect to that of untreated cells (control), and are the mean values ± SEM of three independent experiments, each performed in duplicate. IC_{50} values after 7 days of treatment were calculated from sigmoid dose–response curve (B). The significance of the differences was determined with a one-way ANOVA with Bonferroni post-test: ***$p < 0.001$ vs. control.

*4.2.1. (3Z)-2-((3,4-dimethoxybenzyl)amino)-N-(2-oxo-3-(thiophen-2-ylmethylene) indolin-5-yl)acetamide (**4**)*

The residual material was purified by crystallization from AcOEt/*n*-hexane, affording **4** as the *Z*-isomer (36 mg, 0.08 mmol, 20% yield): mp 167–169 °C. ^{1}H NMR (CDCl3): δ 3.37 (dd, 1H, J = 1.8; 15.1 Hz, CH_2); 3.55 (d, 1H, J = 12.9 Hz, CH_2); 3.75 (d, 1H, J = 15.1 Hz, CH_2); 3.86 (s, 3H, OMe); 3.89 (s, 3H, OMe); 4.00 (d, 1H, J = 12.9 Hz, CH_2); 6.66 (d, 1H, J = 8.2 Hz, Ar); 6.79–6.96 (m, 3H, Ar); 7.11 (dd, 1H, J = 3.6, 5.1 Hz, Ar); 7.32–7.35 (m, 1H, Ar); 7.58 (s, 1H, H-vinyl); 7.62 (d, 1H, J = 5.1 Hz); 7.76 (d, 1H, J = 3.6 Hz, Ar); 8.00 (s, 1H, Ar) ppm. ^{13}C NMR (CDCl3): δ 169.84, 167.85, 148.76, 148.14, 141.84, 137.67, 137.03, 133.48, 128.95, 128.94, 128.93, 128.16, 126.94, 126.09, 124.97, 120.22, 116.49, 111.23, 110.63, 109.22, 78.63, 55.49, 54.44 ppm. Anal. ($C_{24}H_{23}N_3O_4S$) Calc%: C 64.13, H 5.16, N 9.35, S 7.13. Found%: C 64.25, H 5.27, N 9.58, S 7.25.

*4.2.2. (Z)-N-(4-(methylthio)phenyl)-N′-(2-oxo-3-(thiophen-2-ylmethylene)indolin-5-yl)urea (**5**)*

The residual material was purified by crystallization from EtOH, affording **5** as the *Z*-isomer (94 mg, 0.23 mmol, 60% yield): mp 246–248 °C. ^{1}H NMR: δ 2.44 (s, 3H, SMe); 6.78 (d, 1H, J = 8.2 Hz, Ar); 7.11 (d, 1H, *J* = 8.2 Hz, Ar); 7.22 (d, 2H, *J* = 8.4 Hz, Ar); 7.44 (d, 2H, *J* = 8.4 Hz, Ar); 7.84–7.92 (m, 3H, Ar, H-vinyl); 7.96–8.01 (m, 1H, Ar); 8.03 (s, 1H, Ar); 8.48 (br s, 1H); 8.68 (br s, 1H); 10.49 (br s, 1H, NH) ppm. ^{13}C NMR: δ 167.16, 152.65, 137.53, 137.11, 135.69, 133.93, 133.16, 129.54, 127.81, 127.16, 124.93, 121.87, 120.71, 119.91, 118.78, 111.17, 110.27, 109.27, 16.10 ppm. Anal. ($C_{21}H_{17}N_3O_2S_2$) Calc%: C 61.89, H 4.20, N 10.31, S 15.74. Found%: C 61.74, H 4.27, N 10.02, S 15.55.

*4.2.3. (3E)-N-(4-(methylthio)phenyl)-N′-(2-oxo-(3-(1-methyl-1H-imidazol-2-yl)methylene)-indolin-5-yl)urea (**6**)*

The residual material was purified by crystallization from EtOH, affording **6** as the *E*-isomer (101 mg, 0.25 mmol, 64% yield): mp 235–237 °C. ^{1}H NMR: δ 2.43 (s, 3H, SMe); 3.90 (s, 3H, NMe); 6.78 (d, 1H, *J* = 8.3 Hz, Ar); 7.21 (d, 2H, *J* = 8.8 Hz, Ar); 7.36 (s, 2H, Ar); 7.42 (d, 2H, *J* = 8.8 Hz, Ar); 7.53 (s, 1H, H-vinyl); 7.65 (dd, 1H, *J* = 2.0, 8.3 Hz, Ar); 8.49 (br s, 1H); 8.64 (br s, 1H); 9.12 (d, 1H, *J* = 2.0 Hz, Ar); 10.47 (br s, 1H, NH) ppm. ^{13}C NMR: δ 168.27, 157.45, 140.26, 139.14, 137.00, 138.86, 133.66, 130.76, 129.42, 128.27, 127.52, 123.70, 122.84, 121.55, 119.78, 112.57, 108.97; 34.25, 14.20 ppm. Anal. ($C_{21}H_{19}N_5O_2S$) Calc%: C 62.21, H 4.72, N 17.27, S 7.91. Found%: C 62.35, H 4.89, N 17.03, S 8.03.

*4.2.4. (3Z)-N-(4-(methylthio)phenyl)-N′-(2-oxo-(3-(1H-imidazol-5-yl)methylene)indolin-5-yl)urea (**7**)*

The residual material was purified by crystallization from EtOH, affording **7** as the *Z*-isomer (98 mg, 0.25 mmol, 63% yield): mp 215–217 °C. ^{1}H NMR: δ 2.44 (s, 3H, SMe); 6.82 (d, 1H, J = 8.3 Hz, Ar); 7.12 (dd, 1H, J = 1.3, 8.3 Hz, Ar); 7.22 (d, 2H, J = 8.6 Hz, Ar); 7.44 (d, 2H, J = 8.6 Hz, Ar); 7.71 (s, 1H, H-vinyl); 7.79 (s, 1H, Ar); 7.86 (d, 1H, J = 1.3 Hz, Ar); 8.02 (s, 1H, Ar); 8.54 (br s, 1H); 8.70 (br s, 1H); 10.90 (br s, 1H, NH) ppm. ^{13}C NMR: δ 167.58, 153.00, 138.60, 137.01, 135.82, 134.00, 133.27, 128.54, 127.41, 127.03 124.93, 122.07, 120.49, 120.01, 118.58, 111.35, 109.15; 17.18 ppm. Anal. ($C_{20}H_{17}N_5O_2S$) Calc%: C 61.37, H 4.38, N 17.89, S 8.19. Found%: C 61.45, H 4.30, N 18.01, S 8.23.

*4.3. General procedure for the synthesis of compounds **8-10***

A solution of oxone (215 mg, 0.35 mmol) in water was added to a cooled (0 °C) solution of the appropriate derivative **8**–**10** (0.29 mmol) in 1:1 MeOH-THF (2 mL). The resulting mixture was stirred at room temperature for 12 h. Then the solid was filtered off, and the solution was evaporated. The residual material was diluted with MeOH and the solid product was separated out from the mixture. It was filtered, washed with Et_2O, and air dried.

*4.3.1. (3Z)-N-(4-(methylsulfonyl)phenyl)-N′-(2-oxo-3-(thiophen-2-ylmethylene)indolin-5-yl)urea (**8**)*

(76 mg, 0.17 mmol, 60% yield): mp 213–215 °C. ^{1}H NMR: δ 3.16 (s, 3H, SMe); 6.79 (d, 1H, *J* = 8.3 Hz, Ar); 7.14 (d, 1H, *J* = 8.3 Hz, Ar); 7.23 (t, 1H, *J* = 4.3 Hz, Ar); 7.60–7.92 (m, 6H, Ar); 7.98–8.10 (m, 2H, Ar, H-vinyl); 8.75 (br s, 1H); 9.29 (br s, 1H); 10.52 (br s, 1H, NH) ppm. ^{13}C NMR: δ 168.40, 152.56, 148.00, 137.71, 136.09, 134.12, 133.18, 129.54, 127.75, 127.14, 125.03, 121.87, 120.98, 118.94, 118.75, 111.17, 110.27, 109.27; 52.70 ppm. Anal. ($C_{21}H_{17}N_3O_4S_2$) Calc%: C 57.39, H 3.90, N 9.56, S 14.59. Found%: C 57.54, H 4.01, N 10.10, S 14.78.

*4.3.2. (3E)-N-(4-(methylsulfonyl)phenyl)-N′-(2-oxo-3-((1-methyl-1H-imidazol-2-yl)methylene)indolin-5-yl)urea (**9**)*

(79 mg, 0.18 mmol, 62% yield): mp 229–231 °C. ^{1}H NMR: δ 3.15 (s, 3H, SMe); 3.90 (s, 3H, NMe); 6.81 (d, 1H, *J* = 8.2 Hz, Ar); 7.37 (s, 2H,

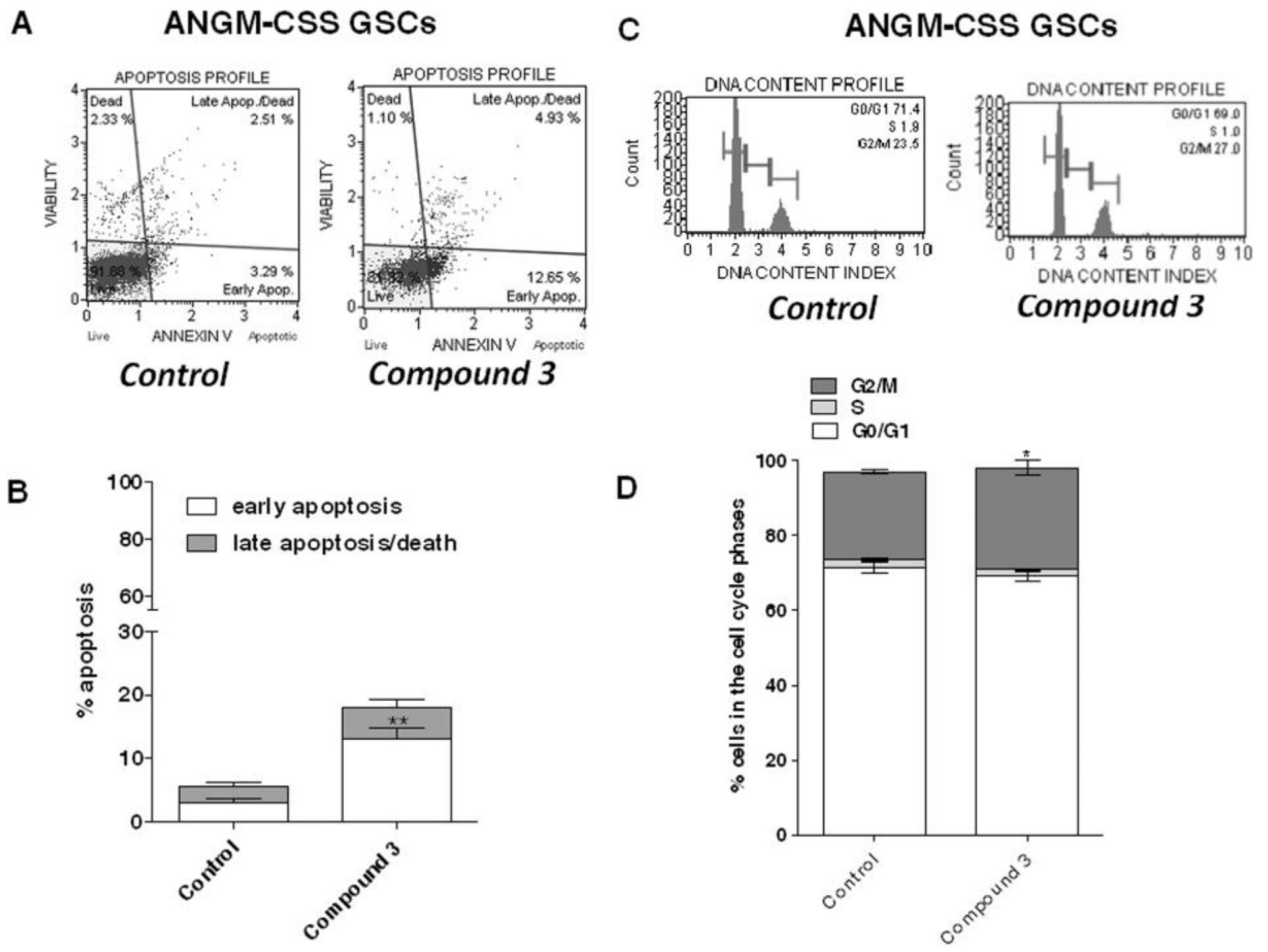

Fig. 5. GSCs were treated for 7 days with NSC medium containing DMSO (control), or 1 μM **3**. At the end of treatments, the cells were collected and the degree of phosphatidylserine externalisation was evaluated using the Annexin V protocol. B) The data were expressed as the percentage of apoptotic cells (early-apoptotic in white, late-apoptotic/necrotic in grey) relative to the total number of cells. C, D) Cell cycle analysis at the end of treatment. The data were expressed as percentage of cell in the different phases (G0/G1, G2 or S) versus total cell number. All the data shown represent the mean ± SEM of three different experiments. The significance of the differences was determined with a one-way ANOVA with Bonferroni post-test: $^{*}p < 0.05$, $^{**}p < 0.01$ vs. control.

Ar); 7.53 (s, 1H, H-vinyl); 7.61–7.71 (m, 3H, Ar); 7.81 (d, 2H, $J = 8.8$ Hz, Ar); 8.70 (br s, 1H); 9.10–9.18 (m, 2H, Ar, NH); 10.51 (br s, 1H, NH) ppm. ^{13}C NMR: δ 168.15, 153.45, 143.56, 139.24, 138.50, 137.86, 134.56, 130.17, 129.71, 128.05, 127.52, 122.73, 122.19, 121.55, 119.53, 112.17, 109.04; 54.25, 35.20 ppm. Anal. ($C_{21}H_{19}N_5O_4S$) Calc%: C 57.66, H 4.38, N 16.01, S 7.33. Found%: C 57.55, H 4.42, N 16.25, S 7.02.

*4.3.3. (3Z)-N-(4-(methylsulfonyl)phenyl)-N′-(2-oxo-3-((1H-imidazol-5-yl)methylene)indolin-5-yl)urea (**10**)*

(75 mg, 0.18 mmol, 61% yield): mp 215–217 °C. ^{1}H NMR: δ 3.16 (s, 3H, SMe); 6.84 (d, 1H, $J = 8.2$ Hz, Ar); 7.15 (d, 1H, $J = 8.3$ Hz, Ar); 7.62–7.85 (m, 6H, H-vinyl, Ar); 7.89 (s, 1H, Ar); 8.02 (s, 1H, Ar); 8.74 (br s, 1H); 9.24 (br s, 1H); 10.93 (br s, 1H, NH) ppm. ^{13}C NMR: δ 168.85, 152.25, 144.49, 139.28, 138.46, 135.20, 133.22, 132.82, 128.01, 127.68 124.50, 122.70, 120.11, 119.45, 117.41, 110.91, 109.73; 55.89 ppm. Anal. ($C_{20}H_{17}N_5O_4S$) Calc%: C 56.73, H 4.05, N 16.54, S 7.57. Found%: C 57.04, H 4.28, N 16.77, S 7.78.

*4.4. Procedure for the synthesis of final compounds **11**–**16***

Compounds **11**–**16** were synthesized from the appropriate 5-substituted-2-oxoindole (0.39 mmol) in EtOH (7 mL) following the same procedure described above for the preparation of compounds **4**–**7**.

*4.4.1. (3Z)-N-(3,4-dimethoxybenzyl)-2-oxo-3-(thiophen-2-ylmethylene)indoline-5-sulfonamide (**11**)*

The residual material was purified by crystallization from EtOH, affording **11** as the *Z*-isomer (110 mg, 0.24 mmol, 62% yield): mp 246–248 °C. ^{1}H NMR: δ 3.62 (s, 6H, OMe); 3.96 (s, 2H, CH_2); 6.68–6.82 (m, 3H, Ar); 6.90 (d, 1H, J = 8.1 Hz, Ar); 7.27 (t, 1H, J = 4.2 Hz, Ar); 7.62 (d, 1H, J = 8.1 Hz, Ar); 7.82–7.94 (m, 1H, Ar); 7.82–7.84 (m, 2H, Ar, NH); 8.04 (s, 1H, H-vinyl); 8.31 (s, 1H, Ar); 10.99 (br s, 1H) ppm. ^{13}C NMR: δ 167.23, 148.39, 147.77, 143.00, 138.66, 137.10, 135.39, 133.36, 130.38, 129.74, 127.65, 127.08, 124.41, 121.53, 119.82, 118.09, 117.69, 111.31, 109.26; 55.40; 55.20; 46.18 ppm. Anal. ($C_{22}H_{20}N_2O_5S_2$) Calc%: C 57.88, H 4.42, N 6.24, S 14.05. Found%: C 58.10, H 4.40, N 6.08, S 14.23.

*4.4.2. (3E)-N-(3,4-dimethoxybenzyl)-3-((1-methyl-1H-imidazol-2yl)methylene)-2- oxoindoline-5-sulfonamide (**12**)*

The residual material was purified by crystallization from EtOH,

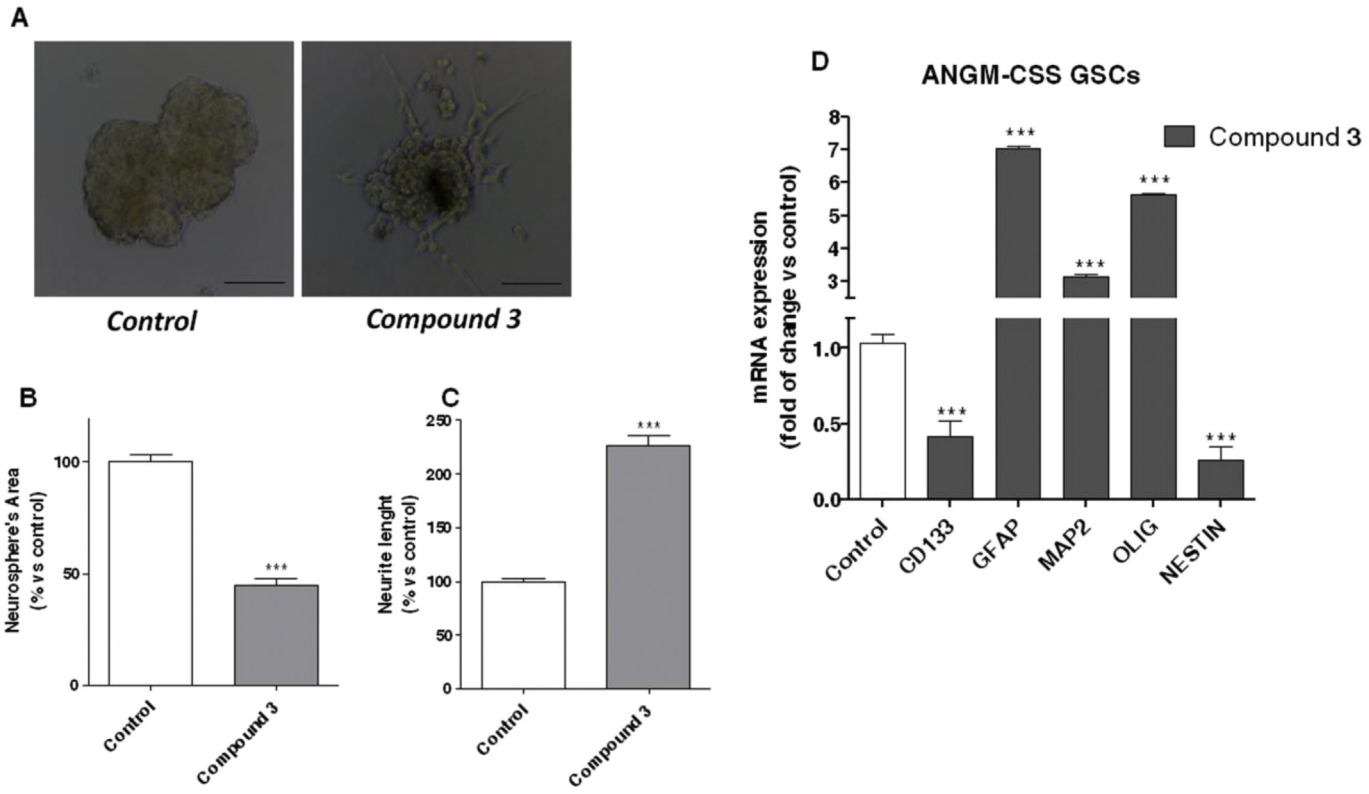

Fig. 6. GSCs were treated for 7 days with complete NSC medium containing DMSO (control), or **3** (1 μM). (A) Representative cell micrographs after 7 days of treatment were shown. (B) The area of the culture plates occupied by the spheres and (C) the length of cellular processes were scored after 7 days of treatment. The counts represent the mean values ± SEM of two independent experiments. (D) GSCs were treated as in A. At the end of treatments, Real time RT-PCR was performed using primer for the stem cell markers CD133 and Nestin, the oligodendrocyte marker Olig, the neuronal marker MAP and for the astrocyte marker GFAP. Data were expressed as fold of change vs the levels of the control (set to 1) and are the mean values ± SEM of three different experiments. The significance of the differences was determined with a one-way ANOVA with Bonferroni post-test: ***$p < 0.001$ vs control.

affording **12** as the *E*-isomer (109 mg, 0.24 mmol, 61% yield): mp 235–237 °C. ^{1}H NMR: δ 3.59 (s, 3H, OMe); 3.67 (s, 3H, OMe); 3.92 (s, 3H, Me); 3.98 (d, 2H, J = 6.1 Hz, CH2); 6.68–6.82 (m, 3H, Ar); 6.96 (d, 1H, J = 8.2 Hz, Ar); 7.39 (s, 1H, Ar); 7.46 (s, 1H, Ar); 7.56 (s, 1H, H-vinyl); 7.68 (dd, 1H, J = 1.8, 8.2 Hz, Ar); 7.92 (br t, 1H, J = 6.1 Hz); 9.92 (d, 1H, J = 1.8 Hz, Ar); 10.99 (br s, 1H) ppm. ^{13}C NMR: δ 169.27, 148.39, 147.77, 145.27, 142.14, 133.73, 130.60, 130.01, 128.59, 125.72, 123.84, 121.53, 119.69, 119.36, 111.57, 108.93; 55.49; 55.18; 46.04; 33.20 ppm. Anal. ($C_{22}H_{22}N_4O_5S$) Calc%: C 58.14, H 4.88, N 12.33, S 7.06. Found%: C 58.02, H 5.16, N 12.06, S 7.30.

*4.4.3. (3Z)-3-(1-(1H-imidazol-5-yl)-ethylidene)-N-(3,4-dimethoxybenzyl)-2-oxoindoline-5-sulfonamide (**13**)*

The residual material was purified by crystallization from EtOH, affording **13** as the *Z*-isomer (110 mg, 0.25 mmol, 64% yield): mp 315–320 °C. ^{1}H NMR: δ 3.34 (s, 6H, OMe); 3.98 (d, 2H, J = 8.1 Hz, CH2); 6.68–6.80 (m, 3H, Ar); 7.02 (d, 1H, J = 8.0 Hz, Ar); 7.40 (s, 1H, Ar); 7.56–7.70 (m, 2H, Ar); 7.80–7.93 (m, 2H, H-vinyl, NH); 8.12 (s, 1H, Ar); 10.00 (br s, 1H) ppm. ^{13}C NMR: δ 168.96, 148.33, 147.73, 143.18, 134.33, 133.73, 133.02, 129.96, 128.58, 127.41, 126.08, 125.63, 124.10, 122.02, 119.82, 111.28, 109.74; 55.45; 55.33; 46.15 ppm. Anal. $C_{21}H_{20}N_4O_5S$) Calc%: C 57.26, H 4.58, N 12.72, S 7.28. Found%: C 57.21, H 4.73, N 12.74, S 7.37.

*4.4.4. (3Z)-N-(2-oxo-(3-(thiophen-2-ylmethylene)indolin-5-yl) methanesulfonamide (**14**)*

The residual material was purified by crystallization from EtOH, affording **14** as the *Z*-isomer (48 mg, 0.15 mmol, 38% yield): mp 185–187 °C. ^{1}H NMR: δ 2.94 (s, 3H, Me); 6.73–6.90 (m, 1H, Ar); 7.00–7.36 (m, 2H, Ar); 7.54 (s, 1H, Ar); 7.79–8.29 (m, 3H, H-vinyl, Ar); 9.38 (br s, 1H); 10.57 (br s, 1H, NH) ppm. ^{13}C NMR: δ 167.09, 137.83, 137.66, 137.01, 134.27, 131.29, 128.47, 127.25, 124.77, 123.46, 121.27, 114.54, 109.60, 38.26 ppm. Anal. ($C_{14}H_{12}N_2O_3S_2$) Calc%: C 52.48, H 3.78, N 8.74, S 20.02. Found%: C 52.64, H 3.66, N 8.89, S 20.24.

*4.4.5. (3E)-N-(2-oxo-(3-(1-methyl-1H-imidazol-2yl)methylene) indolin-5-yl)methanesulfonamide (**15**)*

The residual material was purified by crystallization from EtOH, affording **15** as the *E*-isomer (51 mg, 0.16 mmol, 40% yield): mp 197–199 °C. ^{1}H NMR: δ 2.99 (s, 3H, Me); 3.90 (s, 3H, NMe); 6.82 (d, 1H, *J* = 8.2 Hz, Ar); 7.11 (dd, 1H, *J* = 2.0, 8.2 Hz, Ar); 7.34 (s, 1H, Ar); 7.38 (s, 1H, Ar); 7.52 (s, 1H, H-vinyl); 9.37 (d, 1H, *J* = 2.0 Hz, Ar); 9.42 (br s, 1H); 10.57 (br s, 1H, NH) ppm. ^{13}C NMR: δ 168.92, 139.65, 136.81, 135.45, 131.89, 131.56, 127.46, 123.59, 123.24, 121.13, 117.67, 110.02, 45.07, 38.20 ppm. Anal. ($C_{14}H_{14}N_4O_3S$) Calc%: C 52.82, H 4.43, N 17.60, S 10.07. Found%: C 52.78, H 4.73, N 17.52, S 10.25.

*4.4.6. (3Z)-N-(2-oxo-3-((1H-imidazol-5yl)methylene)indolin-5-yl) methanesulfonamide (**16**)*

The residual material was purified by crystallization from EtOH, affording **16** as the *Z*-isomer (55 mg, 0.18 mmol, 45% yield): mp 205–207 °C. ^{1}H NMR: δ 2.94 (s, 3H, Me); 6.87 (d, 1H, J = 8.1 Hz, Ar); 7.05 (dd, 1H, *J* = 1.7, 8.1 Hz, Ar); 7.50 (d, 1H, *J* = 1.7 Hz, Ar); 7.72 (s, 1H, Ar); 7.83 (s, 1H, Ar); 8.03 (s, 1H, H-vinyl); 9.43 (br s, 1H); 11.02 (br s, 1H, NH) ppm. ^{13}C NMR: δ 170.04, 139.14, 137.77, 131.18, 127.85, 125.79, 123.73, 123.11, 122.29, 114.14, 110.22, 109.17, 38.27 ppm. Anal. ($C_{13}H_{12}N_4O_3S$) Calc%: C 51.31, H 3.97, N 18.41, S 10.54. Found%: C 51.44, H 4.05, N 18.29, S 10.37.

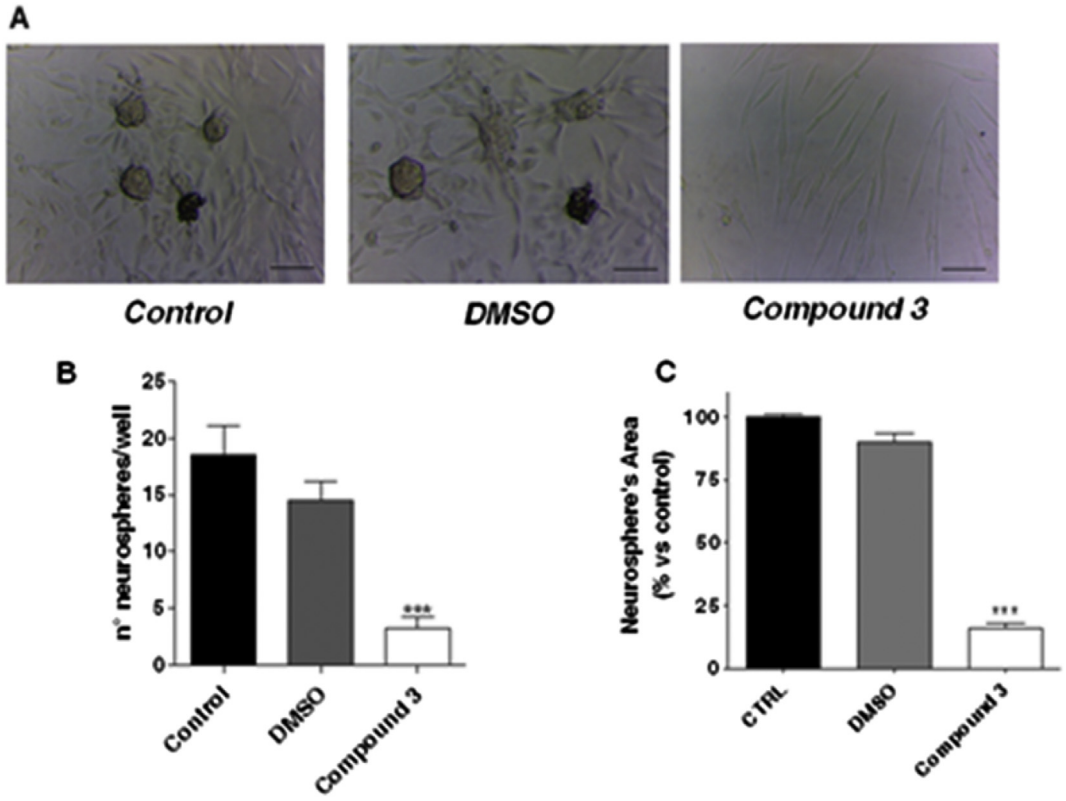

Fig. 7. Effects of 3 on the formation of GSCs. Adherent ANGM-CSS cells were switched to NSC medium, and cells were allowed to growth for 9 days, in the absence or in the presence of 1 μM **3** (**A**) Representative picture of ANGM-CSS neurospheres after 9 days of incubation. The number of the newly formed spheres (**B**) and the mean diameter (**C**) were scored using ImageJ. Data represent the mean ± SEM of three pictures of two independent experiments. The significance of the differences was determined with a one-way ANOVA with Bonferroni post-test: ***$p < 0.001$ vs control.

*4.5. 5-amino-1,3-dihydro-2H-indol-2-one (**17**)*

The commercial 5-nitroindolin-2-one (1.00 g, 5.61 mmol) was hydrogenated in EtOH (70 mL) in the presence of 10% Pd–C (315 mg, 2.97 mmol) for 4 h. Then the catalyst was filtered off through Celite, the Celite rinsed with additional EtOH and the solution was evaporated, to give **17** as a brown solid (698 mg, 4.71 mmol, 84% yield). ^{1}H NMR (CD_3OD): δ 3.43 (s, 2H, CH_2); 6.63–6.65 (m, 2H, Ar); 6.73–6.74 (m, 1H, Ar) ppm. Anal. ($C_8H_8N_2O$) Calc%: C 64.85, H 5.44, N 18.91; Found%: C 65.03, H 5.49, N 18.83.

*4.6. 1-(4-(methylthio)phenyl)-3-(2-oxoindolin-5-yl)urea (**18**)*

To a solution of 5-amino-1,3-dihydro-2H-indol-2-one **17** (148 mg, 1.0 mmol) in 10 mL DCM/MeOH (9:1), 1-isocyanato-4-(methylsulfanyl)benzene (182 mg, 1.1 mmol) was added slowly at 10 °C. The mixture was stirred at the room temperature for 4 h. Solid product **18** was separated out from the mixture. It was filtered, washed with DCM, and air dried. (330 mg, 0.96 mmol, 96% yield): mp 212–214 °C. ^{1}H NMR: δ 2.43 (s, 3H, SMe); 3.52 (s, 2H, CH_2); 6.72 (d, 1H, $J = 8.2$ Hz, Ar); 7.12–7.23 (m, 3H, Ar); 7.37 (s, 1H, Ar); 7.41 (d, 2H, $J = 8.8$ Hz, Ar); 8.48 (br s, 1H); 8.62 (br s, 1H); 10.24 (br s, 1H, NH) ppm. ^{13}C NMR: δ 167.93, 158.66, 145.19, 142.75, 133.57, 129.87, 128.45, 127.67, 126.25, 113.33, 109.09; 108.90; 36.71; 15.10 ppm. Anal. ($C_{16}H_{15}N_3O_2S$) Calc%: C 61.32, H 4.82, N 13.41, S 10.23; Found%: C 61.05, H 4.67, N 13.23, S 10.23.

*4.7. N-(2-oxoindolin-5-yl)methanesulfonamide (**19**)*

To a stirred solution of 5-amino-2-oxindole **17** (148 mg, 1.00 mmol) in H_2O (10 mL) was added MsCl (137 mg, 1.2 mmol) at RT; stirring was continued at room temperature until TLC analysis shows disappearance of the starting material. Then the solution was evaporated to dryness. The residual material was diluted with MeOH and the solid product was filtered out from the mixture, washed with Et_2O, and air dried. (**19**). (86 mg, 0.38 mmol, 38% yield): mp 196–198 °C. ^{1}H NMR: δ 2.88 (s, 3H, Me); 3.47 (s, 2H, CH_2); 6.77 (d, 1H, J = 8.2 Hz, Ar); 7.04 (d, 1H, J = 8.2 Hz, Ar); 7.09 (s, 1H, Ar); 9.37 (br s, 1H); 10.37 (br s, 1H, NH) ppm. ^{13}C NMR: δ 169.74, 135.61, 133.17, 131.18, 126.85, 123.51, 114.84, 112.82, 40.73, 37.41 ppm. Anal. ($C_9H_{10}N_2O_3S$) Calc%: C 47.78, H 4.45, N 12.38, S 14.17; Found%: C 47.91, H 4.68, N 12.51, S 14.28.

*4.8. 2′ -chloro-N-(2-oxo-2,3-dihydro-1H-indol-5-yl)acetamide (**20**)*

To a stirred solution of 5-amino-2-oxindole **17** (122 mg, 0.82 mmol) in acetone (5 mL) and DMF (1.2 mL), cooled at 0 °C, was added dropwise 2-chloroacetyl chloride (93 mg, 0.82 mmol). The reaction mixture was stirred at RT for additional 3 h, then the solvent was evaporated affording derivative **20**, which was used without further purification (180 mg, 0.80 mmol, 98% yield). ^{1}H NMR: δ 3.47 (s, 2H, CH_2); 4.21 (s, 2H, CH_2Cl); 6.73–6.78 (m, 1H, Ar); 7.33 (d, 1H, J = 8.2 Hz, Ar); 7.49 (s, 1H, Ar); 10.15 (br s, 1H, NH); 10.33 (br s, 1H, NH) ppm. ^{13}C NMR: δ 175.92, 163.90, 139.70, 132.22, 125.95, 118.82, 116.61, 108.73, 43.36, 35.90 ppm. Anal. ($C_{10}H_9ClN_2O_2$) Calc%: C 53.47, H 4.04, N 12.47. Found%: C 53.67, H 4.19, N 12.59.

4.9. 2-((3,4-dimethoxybenzyl)amino)-N-(2-oxoindolin-5-yl) acetamide (**21**)

A solution of K_2CO_3 (1.19 g, 8.61 mmol) in CH_3CN (8 mL), heated at 80 °C, was mixed with a solution of compound **20** (879 mg, 3.91 mmol) in DMF (1.3 mL) and with a solution of 3,4-dimethoxybenzylamine (654 mg, 3.91 mmol) in CH_3CN (2 mL). The suspension was stirred at 80 °C for 12 h, then the potassium carbonate was filtered off and the solvent removed. The residue was diluted with CH_2Cl_2 and washed with water and brine. The organic layer was dried and concentrated.

The crude product was purified by crystallization from AcOEt/*n*-hexane, affording compound **21** (462 mg, 1.30 mmol, 33% yield) as a yellow solid. ^{1}H NMR ($CDCl_3$): δ 3.52 (s, 2H, CH_2); 3.78 (s, 2H, CH_2); 3.81 (s, 2H, CH_2); 3.86 (s, 3H, OMe); 3.88 (s, 3H, OMe); 6.76–7.93 (m, 4H, Ar); 7.22 (d, 1H, J = 8.6 Hz, Ar); 7.58 (s, 1H, Ar); 8.02 (br s, 1H, NH); 9.18 (br s, 1H, NH) ppm. ^{13}C NMR ($CDCl_3$): δ 178.05, 169.00, 149.13, 148.86, 139.07, 132.92, 129.16, 125.05, 123.00, 122.55, 120.45, 111.93, 110.66, 56.94, 56.23, 53.70, 51.80, 36.56 ppm. Anal. ($C_{19}H_{21}N_3O_4$) Calc%: C 64.21, H 5.96, N 11.82. Found%: C 63.97, H 5.59, N 11.59.

4.10. Indolin-2-one (**22**)

Iron chips (1.6 g, 29.40 mmol) were added in one portion to commercial 2-nitrophenylacetic acid (2.0 g, 11.04 mmol) in of glacial acetic acid (25 mL). The resulting mixture was heated to 100 °C for 4 h, then concentrated to dryness, sonicated in AcOEt and filtered to remove the insolubles. The filtrate was washed twice with 1 N HCl, H_2O, brine, dried over anhydrous sodium sulfate and concentrated, affording compound **22**. (1.40 g, 10.49 mmol, 95% yield): mp 92–94 °C. ^{1}H NMR ($CDCl_3$): δ 3.56 (s, 2H, CH_2); 6.90 (d, 1H, J = 7.7 Hz, Ar); 6.98–7.06 (m, 1H, Ar); 7.19–7.26 (m, 2H, Ar); 8.95 (br s, 1H) ppm. ^{13}C NMR ($CDCl_3$): δ 179.25, 143.38, 128.54, 125.98, 125.12, 122.93, 110.66; 37.10 ppm. Anal. ($C_8H_7NO_2$) Calc%: C 72.16, H 5.30, N 10.52; Found%: C 72.32, H 5.35, N 10.48.

4.11. 2-oxoindoline-5-sulfonyl chloride (**23**)

Chlorosulfonic acid (27 mL, 408 mmoli) was slowly added dropwise to indolin-2-one **23** (13.3 g, 100 mmol). The reaction temperature was maintained below 30 °C during the addition. Later the reaction mixture was stirred at rt for 1.5 h, and then at 68 °C for 1 h, cooled, and poured carefully into water. The precipitate formed was collected by vacuum filtration, washed with H_2O and dried in a vacuum oven to give compound **23**, which was used without further purification (3.02 g, 13.03 mmol, 98% yield): mp 180–185 °C. 1H NMR: δ 3.46 (s, 2H, CH_2); 6.74 (d, 1H, J = 7.7 Hz, Ar); 7.42–7.46 (m, 2H, Ar); 10.48 (br s, 1H) ppm. ^{13}C NMR: δ 175.89, 143.68, 139.71, 124.55, 121.32, 107.39; 35.16 ppm. Anal. ($C_8H_6ClNO_3S$) Calc%: C 41.48, H 2.61, N 6.05, S 13.84; Found%: C 41.57, H 2.72, N 6.14, S 13.92.

4.12. N-(3,4-dimethoxybenzyl)-2-oxoindoline-5-sulfonamide (**24**)

To a stirred solution of 2-oxoindoline-5-sulfonyl chloride **23** (530 mg, 2.29 mmol) in EtOH (10 mL) was added a solution 3,4-dimethoxybenzylamine (418 mg, 2.50 mmol) in EtOH (2 mL). The suspension was stirred at RT for 4 h, then the mixture was concentrated and the solid collected by vacuum filtration. The residual material was purified by crystallization from MeOH, affording compound **24** (664 mg, 1.83 mmol, 80% yield): mp 227–232 °C. ^{1}H NMR: δ 3.52 (s, 2H, CH_2); 3.65 (s, 3H, OMe); 3.69 (s, 3H, OMe); 3.88 (d, 1H, J = 6.2 Hz, CH_2); 6.68–6.82 (m, 3H, Ar); 6.90 (d, 1H, J = 8.1 Hz, Ar); 7.51 (s, 1H, Ar); 7.60 (d, 1H, J = 8.1 Hz, Ar); 7.89 (br t, 1H, J = 6.2 Hz); 10.76 (br s, 1H) ppm. ^{13}C NMR: δ 168.20, 148.35, 147.75, 143.02, 134.39, 133.50, 128.04, 127.67, 126.08, 122.41, 111.89, 111.31, 109.46; 55.49; 55.20; 46.10; 34.10 ppm. Anal. ($C_{17}H_{18}N_2O_5S$) Calc%: C 56.43, H 5.01, N 7.73, S 8.85; Found%: C 56.26, H 5.32, N 7.80, S 8.92.

4.13. Molecular descriptor calculation

Molecular descriptors related to ADME and drug-likeness properties of the investigated compounds were calculated by using publicly available software. In particular, the following descriptors: MW, nHBA, nHBD, nRotB, nRotBt, and Lipinski Failures were calculated with PaDEL Descriptor [20]; LogP, LogD, TPSA, and pKa were calculated with ChemAxon MarvinSketch 6.3.0 [21]; CNS MPO was calculated according to Wager et al. [22].

5. In vitro biological studies

5.1. Cell lines

The human AsPC1 cell line derived from human pancreatic adenocarcinoma. Cells were grown in RPMI-1640 with 10% fetal bovine serum, 1% glutamine and 1% penicillin–streptomycin (Sigma–Aldrich). Cells were cultured in Petri dishes at 37 °C in 5% CO_2 and 95% air. U118MG and ANGM-CSS cell lines, derived from human glioblastoma (ATCC, Manassas, VA, USA and IRCCS-CASA, Sollievo Della Sofferenza Hospital, San Giovanni Rotondo, FG, Italy), were both cultured in DMEM:HAMS F12 (1:1) (Sigma–Aldrich) supplemented with 2 mM of L-glutamine (Sigma Aldrich), 10% Fetal Bovine Serum (FBS, Sigma–Aldrich), 100 units/ml penicillin and 100 μg/ml streptomycin (P/S) in tissue culture flasks at 37 °C in a humidified atmosphere of 5% CO_2.

5.1.1. Cell proliferation assay on ASPC1

Cells were plated in 12-well sterile plastic plates, allowed to attach for 24 h, and then treated in duplicate with indicated compounds at 10 μM. After 72 h, the number of viable cells was assessed by manual cell counting. Changes in cell growth were expressed as a percentage relative to cells treated with DMSO (control).

5.1.2. Z'Lyte assay on selected kinases

The assay was performed by Invitrogen corporation on AKT1 (PKB alpha), PDK1 direct, CHK1, GSK3A and GS3KB as reported below: (AKT1) The 2× AKT1 (PKB alpha)/Ser/Thr 06 mixture is prepared in 50 mM HEPES pH 7.5, 0.01% BRIJ-35, 10 mM $MgCl_2$, 1 mM EGTA. The final 10 μL kinase reaction consists of 1.15–25 ng AKT1 (PKB alpha) and 2 μM Ser/Thr 06 in 50 mM HEPES pH 7.5, 0.01% BRIJ-35, 10 mM $MgCl_2$, 1 mM EGTA. After the 1 h kinase reaction incubation, 5 μL of a 1:2048 dilution of Development Reagent A is added. (PDK1 Direct) The 2× PDK1 Direct/Ser/Thr 07 mixture is prepared in 50 mM Tris pH 8.5, 0.01% BRIJ-35, 10 mM MgCl2, 1 mM EGTA, 0.02% NaN3. The final 10 μL kinase reaction consists of 7.36–38.7 ng PDK1 Direct and 2 μM Ser/Thr 07 in 50 mM Tris/HEPES pH 8.0, 0.01% BRIJ-35, 10 mM $MgCl_2$, 1 mM EGTA, 0.01% NaN_3. After the 1 h kinase reaction incubation, 5 μL of a 1:32,768 dilution of development reagent A is added. CHEK1 (CHK1): The 2× CHEK1 (CHK1)/Ser/Thr 19 mixture is prepared in 50 mM HEPES pH 7.5, 0.01% BRIJ-35, 10 mM $MgCl_2$, 1 mM EGTA. The final 10 μL Kinase Reaction consists of 2.04–35 ng CHEK1 (CHK1) and 2 μM Ser/Thr 19 in 50 mM HEPES pH 7.5, 0.01% BRIJ-35, 10 mM MgCl2, 1 mM EGTA. After the 1 h Kinase Reaction incubation, 5 μL of a 1:256 dilution of Development Reagent A is added. GSK3A (GSK3 alpha): The 2× GSK3A (GSK3 alpha)/Ser/Thr 09 mixture is prepared in 50 mM HEPES pH 7.5, 0.01% BRIJ-35, 10 mM MgCl2, 1 mM EGTA. The final 10 μL Kinase Reaction consists of 0.21–1.69 ng GSK3A (GSK3 alpha)

and 2 μM Ser/Thr 09 in 50 mM HEPES pH 7.5, 0.01% BRIJ-35, 10 mM MgCl2, 1 mM EGTA. After the 1 h Kinase Reaction incubation, 5 μL of a 1:512 dilution of Development Reagent A is added. GSK3B (GSK3 beta): The 2× GSK3B (GSK3 beta)/Ser/Thr 09 mixture is prepared in 50 mM HEPES pH 7.5, 0.01% BRIJ-35, 10 mM MgCl2, 1 mM EGTA. The final 10 μL Kinase Reaction consists of 0.17–0.88 ng GSK3B (GSK3 beta) and 2 μM Ser/Thr 09 in 50 mM HEPES pH 7.5, 0.01% BRIJ-35, 10 mM MgCl2, 1 mM EGTA. After the 1 h Kinase Reaction incubation, 5 μL of a 1:512 dilution of Development Reagent A is added.

5.1.3. Protein kinase profiling

Effect of the indicated compounds on the activity of various kinases was assessed by SelectScreen Kinase Profiling Service (Invitrogen-Life Technologies, Paisley, UK). Assays were performed using 1uM of compound **3** and ATP concentration as indicated in the corresponding table.

5.1.4. Cell proliferation assay on ANGM-CSS and U118MG

Cells were cultured up to about 80% confluence in culture medium and 24 h before the experiment, cells were seeded onto 96-well plates at a density per well of 10^3 for U118MG and 3×10^3 for ANGM-CSS (only for U118MG it was necessary to pre-coat every well with gelatine 1% from porcine skin, Sigma–Aldrich). After 24 h to allow cell attachment, the medium was replaced in each 96-well plate and the cells were treated for 72 h, 96 h, 120 h and 144 h with G51 compound (40 μM, 20 μM, 10 μM, 5 μM and 2.5 μM), vehicle (DMSO 0.1%) or control (no-treatment). At the end of each treatments cell viability was assessed using the Cell Proliferation Reagent WST-1 (4-[3-(4-iodophenyl)-2-(4-nitrophenyl)-2*H*-5-tetrazolium]-1,3-benzene disulphonate) (Roche, Mannheim, Germany) based on the cellular cleavage of the WST-1 to formazan. WST-1 was added at 1/10 of the total volume and after 60 min of incubation at 37 °C, the absorbance was measured at 450 nm with a multiplate reader (Enspire; PerkinElmer, Wellesley, MA, USA).

5.1.5. GSC isolation from ANGM-CSS cells

To obtain the GSC subpopulation, approximately 2.0×10^6 ANGM-CSS cells were suspended in 1 mL of a defined serum-free Neural Stem Cell (NSC) medium [33]. After 5–6 days of culture, GSCs (called "neurospheres") were collected, suspended in NSC medium, dissociated into single cells and plated for the assays. The method accuracy for GSC isolation was verified in previous experiments [19,33]. For the long-term treatment of cells, NSC or complete medium containing drugs was replaced every two to three days.

5.1.6. Cell proliferation assays on GSCs

GSCs were seeded at a density of 3×10^4 cells/well in 24 well-plate, and then treated from one to seven days with fresh growth medium containing different concentrations of compound **3** (0.1 nM–100 μM). Following the treatment period, GSCs were collected and transferred in 96 well-plate, and cell proliferation was determined using the MTS assay according to manufacturer's instruction. The absorbance of formazan at 490 nM was measured in a colorimetric assay with an automated plate reader (Victor Wallac 2, Perkin Elmer). The results were calculated by subtracting the mean background from the values obtained from each evaluation and were expressed as the percentage of the control (untreated cells). Sigmoid dose–response curve was generated, from which the IC_{50} values were derived.

5.1.7. Annexin V and 7-AAD staining in ANGM-CSS cells and in GSCs

Dual staining with Annexin V coniugated to fluorescein-isothiocyanate (FITC) and 7-amino-actinomysin (7-AAD) was performed using the commercially available kit (Muse Annexin V and Dead Cell Kit; Merck KGaA, Darmstadt, Germany). ANGM-CSS cells or GSCs were treated with DMSO (control) or compound **3** (1 μM) for 72 h or seven days, respectively. At the end of the treatment periods, the percentages of living, apoptotic and dead cells were acquired and analyzed by Muse™ Cell Analyzer as previously described [19].

5.1.8. Cell cycle analysis in ANGM-CSS cells and in GSCs

The measurement of the percentage of cells in the different cell phases was performed using the Muse™ Cell Analyzer (Merck KGaA, Darmstadt, Germany). Briefly, U87MG or GSCs were treated with DMSO or compound **3** (1 μM), for 72 h or seven days, respectively. Cells were collected and centrifuged at 300 × g for 5 min. The pellets were washed with PBS and suspended in 100 μl of PBS, and cells were slowly added to 1 mL of ice cold 70% ethanol and maintained o/n at −20 °C. Then, a cell suspension aliquot (containing at least 2 × 105 cells) was centrifuged at 300 × g for 5 min, washed once with PBS and suspended in the fluorescent reagent (Muse™ Cell Cycle reagent) [34].

5.1.9. RNA extraction and Real Time PCR analysis in GSCs

GSCs were treated with DMSO (control), or different concentrations of compound **3** (1 nM–1μM) for seven days. At the end of treatments, cells were collected, and total RNA was extracted using Rneasy® Mini Kit (Qiagen, Hilden, Germany) according to manufacturer's instructions. cDNA synthesis was performed with 500 ng of RNA using i-Script cDNA synthesis kit (BioRad, Hercules, USA) following manufacturer's instructions. RT-PCR reactions consisted of 25 μL Fluocycle® II SYBR® (Euroclone, Milan, Italy), 1.5 μL of both 10 μM forward and reverse primers, 3 μL cDNA, and 19 μL of H_2O. All reactions were performed for 40 cycles using the following temperature profiles: 98 °C for 30 s (initial denaturation); T °C (see Table S2) for 30 s (annealing); and 72 °C for 3 s (extension) [33].

5.1.10. Quantitation of the occupied area and the cellular processes of neurospheres

GSCs were plated in complete growth medium (day 0) and treated for the indicated days with compound **3**. Photographs of the neurospheres were taken at days 0, 7, and 21. Three different wells were analyzed for each condition, and 15 images of each well were captured [19,33]. The response of the cultures to the various treatments was quantified by measuring the area occupied by neurospheres that had formed, using the Image J program (version 1.41; Bethesda, MD, USA). The cellular processes extending from the six to eight differentiating neurospheres per condition in three independent experiments were evaluated.

5.1.11. Neurosphere formation assay

The ability of ANGM-CSS to initiate neurosphere formation were assessed by harvesting, washing, and resuspending monolayer cells in serum-free NSC medium. Cells were seeded into 96-well at 2×10^4 cells/well and incubated with DMSO (0.5%, control) or compound **3** (1 μM) for 9 days without disturbing the plates, and without replenishing the medium. At the end of the treatment period, pictures of the neurospheres were taken. Three different wells were analyzed for each condition and 3 images of each well were captured. The number and the diameter of the newly formed neurosphere were estimated using the Image J program (version 1.41; Bethesda, MD, USA).

6. Statistical analysis

All the experiments were performed in duplicate and repeated three times. ASPC1 data were expressed as mean values ± S.D. and analyzed by Student's t test; the level of significance was set at $P < 0.05$.

The nonlinear multipurpose curve-fitting program Graph-Pad Prism (GraphPad Software Inc., San Diego, CA) was used for data analysis and graphic presentations. All data are presented as the mean ± SEM. Statistical analysis was performed by one-way analysis of variance (ANOVA) with Bonferroni's corrected t-test for post-hoc pair-wise comparisons. $P < 0.05$ was considered statistically significant. The parameter of GI_{50} was calculated as the molar concentration of the tested compound evoking a half reduction in cell viability.

Acknowledgment

We thank the International Society for Drug Development (ISDD, Milano) who partially supported this research. The authors declare no competing financial interest.

Appendix A. Supplementary data

Supplementary data related to this article can be found at http://dx.doi.org/10.1016/j.ejmech.2015.10.020.

References

[1] T.A. Wilson, M.A. Karajannis, D.H. Harter, Glioblastoma multiforme: state of the art and future therapeutics, Surg. Neurol. Int. 5 (2014) 64.
[2] P. Kleihues, W. Cavanee, World Health Organization Classification of Tumors: Pathology and Genetic: Tumors of the Nervous System, IARC, Press, 2000 (Ref Type: Generic).
[3] A. Behin, et al., Primary brain tumours in adults, Lancet 361 (9354) (2003) 323–331.
[4] R. Stupp, et al., Effects of radiotherapy with concomitant and adjuvant temozolomide versus radiotherapy alone on survival in glioblastoma in a randomised phase III study: 5-year analysis of the EORTC-NCIC trial, Lancet Oncol. 10 (5) (2009) 459–466.
[5] S. Colak, J.P. Medema, Cancer stem cells–important players in tumor therapy resistance, FEBS J. 281 (21) (2014) 4779–4791.
[6] A. Eramo, et al., Chemotherapy resistance of glioblastoma stem cells, Cell Death Differ. 13 (7) (2006) 1238–1241.
[7] S. Bao, et al., Glioma stem cells promote radioresistance by preferential activation of the DNA damage response, Nature 444 (7120) (2006) 756–760.
[8] A. Shervington, C. Lu, Expression of multidrug resistance genes in normal and cancer stem cells, Cancer Investig. 26 (5) (2008) 535–542.
[9] D. Chen, et al., Discovery of potent N-(isoxazol-5-yl) amides as HSP90 inhibitors, Eur. J. Med. Chem. 87 (2014) 765–781.
[10] I. Vivanco, C.L. Sawyers, The phosphatidylinositol 3-kinase–AKT pathway in human cancer, Nat. Rev. Cancer 2 (7) (2002) 489–501.
[11] P.Y. Wen, et al., Current clinical development of PI3K pathway inhibitors in glioblastoma, Neuro-oncology 14 (7) (2012) 819–829.
[12] K. Shih, et al., Phase I study of the combination of BKM120 and bevacizumab in patients with relapsed/refractory glioblastoma multiforme (GBM) or other refractory solid tumors, in: ASCO Meeting Abstracts, 2013.
[13] X. Ma, Y. Hu, Targeting PI3K/Akt/mTOR cascade: the medicinal potential, updated research highlights and challenges ahead, Curr. Med. Chem. 20 (24) (2013) 2991–3010.
[14] G. Nesi, et al., Synthesis of novel 3,5-disubstituted-2-oxindole derivatives as antitumor agents against human nonsmall cell lung cancer, ACS Med. Chem. Lett. 4 (12) (2013) 1137–1141.
[15] M.D.M. AbdulHameed, et al., Combined 3D-QSAR modeling and molecular docking study on indolinone derivatives as inhibitors of 3-phosphoinositide-dependent protein kinase-1, J. Chem. Inf. Model. 48 (9) (2008) 1760–1772.
[16] I. Islam, et al., Indolinone based phosphoinositide-dependent kinase-1 (PDK1) inhibitors. Part 1: design, synthesis and biological activity, Bioorg. Med. Chem. Lett. 17 (14) (2007) 3814–3818.
[17] I. Islam, et al., Indolinone based phosphoinositide-dependent kinase-1 (PDK1) inhibitors. Part 2: optimization of BX-517, Bioorg. Med. Chem. Lett. 17 (14) (2007) 3819–3825.
[18] A. Notarangelo, et al., Establishment and genetic characterization of ANGM-CSS, a novel, immortal cell line derived from a human glioblastoma multiforme, Int. J. Oncol. 44 (3) (2014) 717–724.
[19] S. Daniele, et al., Combined inhibition of AKT/mTOR and MDM2 enhances glioblastoma multiforme cell apoptosis and differentiation of cancer stem cells, Sci. Rep. 5 (2015).
[20] C.W. Yap, PaDEL-descriptor: an open source software to calculate molecular descriptors and fingerprints, J. Comput. Chem. 32 (7) (2011) 1466–1474.
[21] I.V. Tetko, et al., Virtual computational chemistry laboratory–design and description, J. Computer-aided Mol. Des. 19 (6) (2005) 453–463.
[22] T.T. Wager, et al., Moving beyond rules: the development of a central nervous system multiparameter optimization (CNS MPO) approach to enable alignment of druglike properties, ACS Chem. Neurosci. 1 (6) (2010) 435–449.
[23] D.E. Clark, *In silico* prediction of blood–brain barrier permeation, Drug Discov. Today 8 (20) (2003) 927–933.
[24] L. Sun, et al., Design, synthesis, and evaluations of substituted 3-[(3-or 4-carboxyethylpyrrol-2-yl) methylidenyl] indolin-2-ones as inhibitors of VEGF, FGF, and PDGF receptor tyrosine kinases, J. Med. Chem. 42 (25) (1999) 5120–5130.
[25] L. Sun, et al., Synthesis and biological evaluations of 3-substituted indolin-2-ones: a novel class of tyrosine kinase inhibitors that exhibit selectivity toward particular receptor tyrosine kinases, J. Med. Chem. 41 (14) (1998) 2588–2603.
[26] T. Asano, et al., The PI 3-kinase/Akt signaling pathway is activated due to aberrant pten expression and targets transcription factors NF-κB and c-Myc in pancreatic cancer cells, Oncogene 23 (53) (2004) 8571–8580.
[27] I. Murtaza, et al., Suppression of cFLIP by lupeol, a dietary triterpene, is sufficient to overcome resistance to TRAIL-mediated apoptosis in chemoresistant human pancreatic cancer cells, Cancer Res. 69 (3) (2009) 1156–1165.
[28] E.A. Jares-Erijman, T.M. Jovin, FRET imaging, Nat. Biotechnol. 21 (11) (2003) 1387–1395.
[29] M. Verreault, et al., Combined RNAi-mediated suppression of rictor and EGFR resulted in complete tumor regression in an orthotopic glioblastoma tumor model, PloS One 8 (3) (2013) e59597.
[30] K. Nagashima, et al., Genetic and pharmacological inhibition of PDK1 in cancer cells characterization of a selective allosteric kinase inhibitor, J. Biol. Chem. 286 (8) (2011) 6433–6448.
[31] S. Korur, et al., GSK3β regulates differentiation and growth arrest in glioblastoma, PloS One 4 (10) (2009) e7443.
[32] M. Signore, et al., Combined PDK1 and CHK1 inhibition is required to kill glioblastoma stem-like cells in vitro and in vivo, Cell Death Dis. 5 (2013) e1223–e1223.
[33] S. Daniele, et al., Modulation of A1 and A2B adenosine receptor activity: a new strategy to sensitise glioblastoma stem cells to chemotherapy, Cell Death Dis. 5 (11) (2014) e1539.
[34] S. Daniele, et al., Apoptosis therapy in cancer: the first single-molecule co-activating p53 and the translocator protein in glioblastoma, Sci. Rep. 4 (2014).